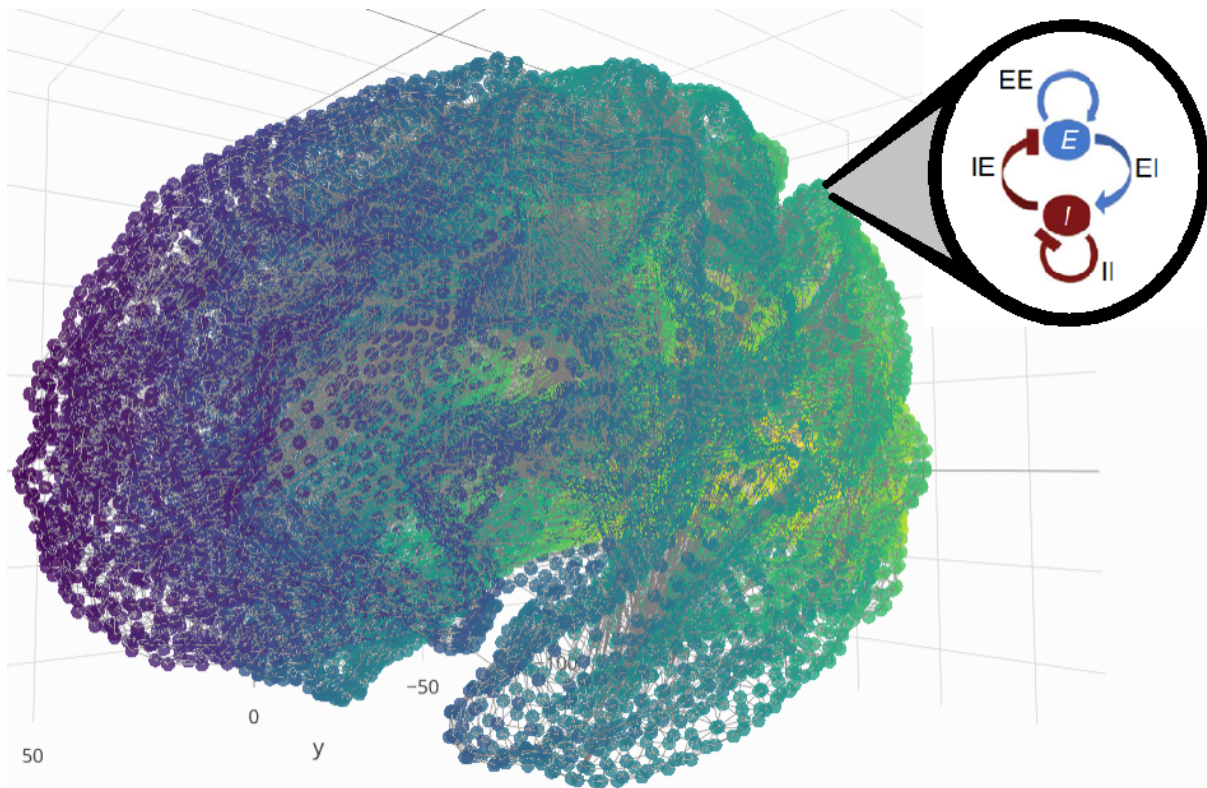

A GRAPH-THEORETIC FRAMEWORK FOR NEURAL FIELD MODELS ON THE HUMAN CONNECTOME

Marco Aqil, Master's Thesis.

Supervisor: Rikkert Hindriks



Abstract. — In this work, we describe a mathematical framework based on the metric graph Laplacian, allowing the implementation of a large family of neural field models on graphs. As an example, we study a stochastic Wilson-Cowan model on a human connectome graph with 18755 cortical vertices and 63260 edges, including both intra-cortical connections, and cortico-cortical white matter tracts. Resting state brain activity is modeled as noise-induced equilibrium fluctuations about a steady state, with parameter choice guided by a qualitative comparison with empirical fMRI data. The main analytic results are a connectome-wide prediction for the 2D spatiotemporal power spectrum of neural activity, and its functional connectivity. Numerical results include nonlinear simulations on a regular one-dimensional graph, and simulations of the linearized model on the full human connectome, both showing excellent agreement of spatiotemporal measures with the analytic predictions. The framework allows in-depth study of model dynamics arising from the underlying anatomical structure, and comparison with empirical data from different functional neuroimaging modalities in health and pathology. It may therefore be used to test and develop new theoretical models and analysis methods of neural activity.

Popular Summary

A major question in modern neuroscience is how cognitive functional abilities arise from the underlying anatomical structure of the human brain (the "connectome"). Dynamic electrochemical neural activity is considered the main biophysical correlate of any cognitive process taking place in the brain. But what theoretical principles allow neural activity to spontaneously self-organize into such a computationally efficient and complex system? Neural field theory seeks to find an answer to this question by developing simplified models of neural activity, amenable to mathematical and computational analysis, but that should nonetheless capture the crucial properties of the system. Such models, essentially coupled integrodifferential equations, approximate the human cortex with simplified geometries (flat or spherical surfaces), and might represent a bridge between structure and function. An alternative approach is that of neural mass models, which describe instead discrete, coupled networks of macroscopic brain regions. In this thesis, we develop an intermediate approach, based on the "graph Laplacian" matrix, an important concept in graph theory. The graph Laplacian matrix captures the anatomical structure of the system, and can be used to directly implement neural field models on a high-resolution human connectome. We study the spatiotemporal properties of an exemplar case (the "Wilson-Cowan" model) with a combination of analysis, numerical simulations, and comparison with empirical data. We conclude that the graph Laplacian formalism may be useful to develop and test new models and analysis methods of neural activity.

Contents

Popular Summary	3
1. Introduction	5
1.1. The Structure-Function Relation	5
1.2. Large Scale Models of Brain Activity	5
2. From Neural Fields to Neural Dynamics on Graphs	9
2.1. Neural Field Theory	9
2.2. The Wilson-Cowan Model	10
3. The Graph Laplacian Framework	12
3.1. The Metric Graph Laplacian	12
3.2. Spatial Convolution Integrals on Graphs	14
3.3. Time Evolution Operators on Graphs	18
4. The Wilson-Cowan Model on Graphs	22
4.1. Mathematical Formulation	22
4.2. Linear Stability Analysis	23
5. Equilibrium Fluctuations in the Stochastic Wilson-Cowan Model on Graphs	28
5.1. Spatiotemporal Power Spectrum	28
5.2. Functional Connectivity	30
5.3. Comparison with Empirical Data	30
6. Numerical Simulations of the Stochastic Wilson-Cowan Model on Graphs	32
6.1. Nonlinear Simulations on a Regular One-Dimensional Graph	32
6.2. Linearized Simulations on the Human Connectome Graph	32
7. Discussion	34
7.1. The Wilson-Cowan Model of Atasoy et al.	34
7.2. Neural Mass Models	34
7.3. Neural Field Models	35
7.4. Limitations	35
8. Conclusion and Future Work	36
Appendix	38
A.1 Spatial Power Spectrum with Ornstein-Uhlenbeck Method	38
A.2 Spatiotemporal Power Spectrum of the Continuous Diffusion Equation	39
A.3 Code	41
Acknowledgements	42
References	43

1. Introduction

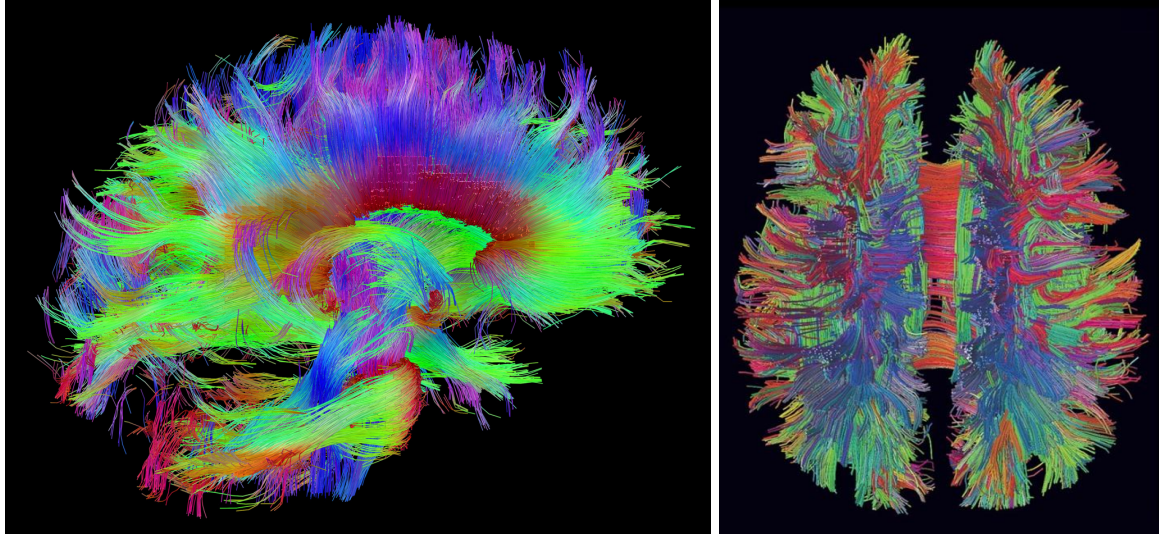


FIGURE 1. The human structural connectome, showing intrahemispheric and interhemispheric white matter tracts.

1.1. The Structure-Function Relation. — In recent years, vast amounts of evidence have been accumulating in favor of the claim that brain activity at rest - that is, in the absence of internal cognitive tasks or external stimuli - is not random, as one might be inclined to think, but actually follows specific patterns [16] which are discernible by fMRI and other neuroimaging methods. These patterns of activity have been related to brain networks known to play functional roles in cognitive tasks, and therefore dubbed "Resting State Networks" (RSNs). Resting state activity is strongly constrained by the underlying anatomical structure (the connectome), but cannot be directly predicted from it in any trivial way: in particular, it is known that structural connections imply functional ones, but the converse is not true [16]; and furthermore, specific discordant attributes of structural and functional connectivity have been found by network analyses [28]. Investigating this relation is a crucial aspect of the "structure-function" problem in neuroscience, that is the question of how the dynamic functional activity and cognitive capabilities of the human brain arise from the underlying anatomy. Nonetheless, despite the intrinsic difficulties inherent in investigating a multi-scale and remarkably complex system such as the human brain, much progress has been achieved in capturing different aspects of the structure-function relation, with varying degree of success, at different scales [5, 27, 39].

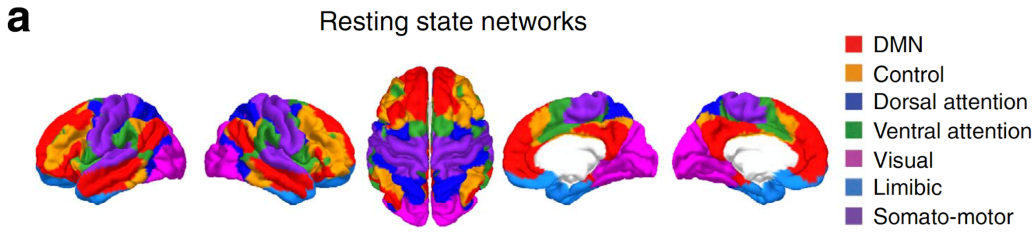


FIGURE 2. Anatomy of the human Resting State Networks. Figure from [3]

1.2. Large Scale Models of Brain Activity. — In order to discuss the advantages and disadvantages of our approach, it is important to situate it within the existing landscape of large-scale brain activity studies. In this context, it is often possible to distinguish between more data-driven ("analysis") and theory-driven ("modeling") approaches, although many of the most recent studies straddle

the boundary between the two. Roughly speaking, in the former case, mathematical/computational analysis is carried out directly on the functional neuroimaging data, with tools from signal processing [26], graph theory [28], or more recently algebraic topology [33], in order to extract relevant cognitive information, or a relation to the underlying anatomy. In the latter type of approach instead, as summarized in the excellent review by Breakspear [8], the work begins with theoretical and biophysical considerations, which are employed to devise a simplified model of neural activity (for example, discrete coupled oscillators, or continuous reaction-diffusion systems), in an attempt to gain insight into the theoretical constraints on the organization of functional activity on the connectome.

Within the theory-driven, whole-brain modeling approaches, an important distinction can be drawn between *neural mass models*, and *neural field models*. In neural mass models, e.g. [17] (Figure 3), cortical activity is usually modeled through networks of a few tens or hundreds of discrete coupled objects, simple oscillators or more complex dynamical systems incorporating biophysical features, each representing local mesoscopic dynamics of neuronal populations. In neural field models, e.g. [35] (see Section 2.1 and Figure 5), brain activity is modeled with a set of integrodifferential equations on a continuous, two-dimensional surface (most commonly a flat sheet or the surface of a sphere), and in some cases, additional mathematical techniques are used to relate activity dynamics on the simplified geometry to the folded cortex. Other authors, for example Spiegler and Jirsa [43], have offered intermediate approaches, which can "translate" between neural fields and neural masses. Our work can be contextualized most appropriately among these latter theory-driven, intermediate approaches, since it can be interpreted both from the perspective of neural fields and of neural masses.

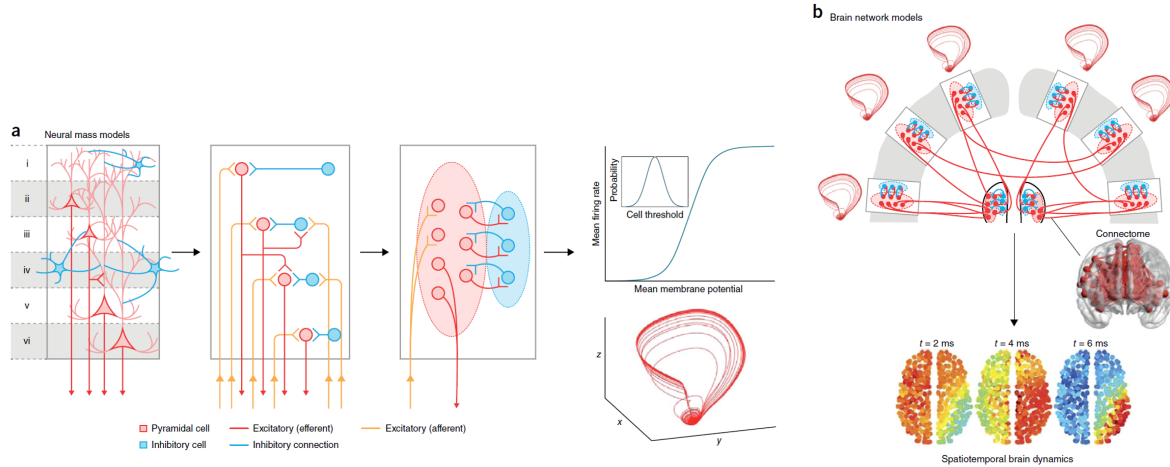


FIGURE 3. Example of a whole-brain activity model. (a) The activity of individual neurons is averaged into the dynamics of local *neural masses*, often comprising of excitatory and inhibitory populations. (b) Local populations are then coupled in a network reflecting structural anatomy to obtain whole-brain activity. Figure adapted from [8].

1.2.1. "Connectome Harmonics" and Beyond. — Among the many analysis methods, mathematical-computational models, and theoretical frameworks proposed, a particularly interesting approach is that of Atasoy et al. [3], based on the *graph-Laplacian* formalism. The graph Laplacian is defined through the adjacency matrix of the graph (see Section 3 for details), and is a symmetric, graph-specific matrix, which serves as the graph-theoretic analogue of the continuous Laplacian operator. The concept and properties of the graph Laplacian, together with its extensions (e.g. the fractional graph-Laplacians), have been explored in the context of spectral theory [30], partial difference equations [20], signal processing on graphs [41], and even machine learning theory [20]. However, few applications to neural field modeling have so far been proposed, with the first instance (to our knowledge) being [3]. Treating the human structural connectome as a graph, Atasoy et al. calculate the eigenvectors of the graph-Laplacian matrix, dubbed "connectome harmonics" by analogy with the famous harmonic patterns that are eigenfunctions of the continuous Laplacian, objects appearing ubiquitously in physics and applied mathematics because they are also the basis of the Fourier transform. Neural activity can therefore be decomposed and studied in this connectome-harmonic basis. Atasoy et al. then proceed

to show how some connectome harmonics are significantly related to human resting state networks, paving the way for a graph-Laplacian based approach to the structure-function question. Furthermore, Atasoy et al. employ the graph Laplacian to implement a deterministic Wilson-Cowan [14] neural field model on the human connectome, and study it with linear stability analysis and numerical simulations. They show that, in some regions of the model parameter space, a Turing instability generated by the interplay of excitatory and inhibitory neuronal populations would lead to dynamic self-organization of connectome-harmonic patterns of activity related to RSNs. Despite limitations and minor technical flaws in the analysis of the model, this approach appeared as a potentially promising area for further exploration in terms of mathematical analysis and computational modeling. In fact, the work of Atasoy et al. has already been cited in dozens of studies and followed up by several different groups (of particular note [45], where a multi-kernel learning strategy is devised to relate structural and functional connectivity).

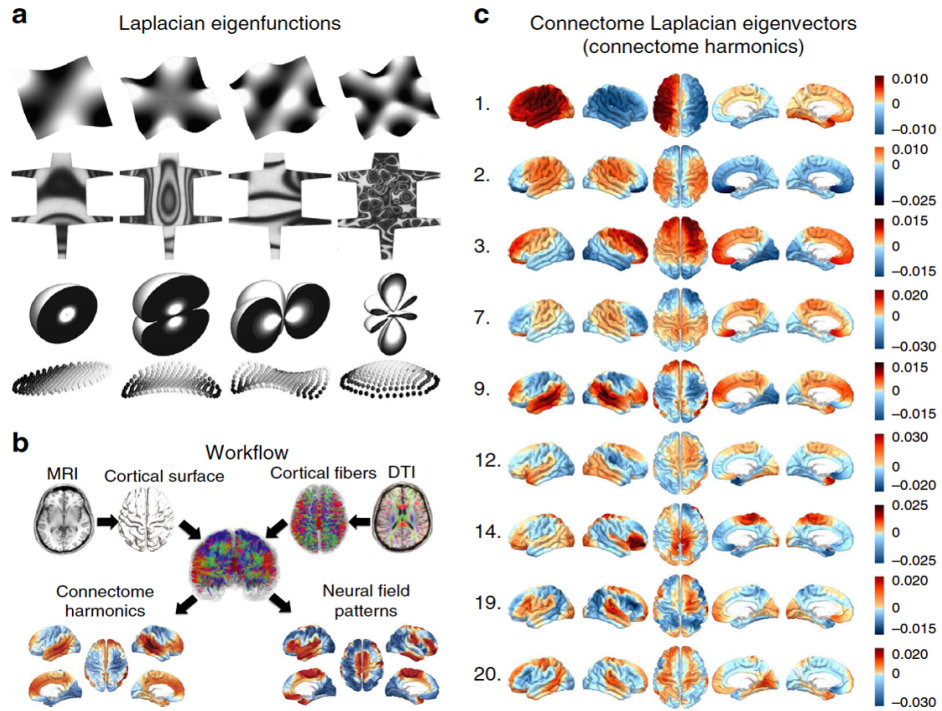


FIGURE 4. (a) The continuous Laplacian operator eigenfunctions on different geometries. (b) Construction of the structural connectome from MRI and DTI data. (c) Eigenvectors of the connectome graph Laplacian. Atasoy et al. proposed them to be self-organizing neural activity building-blocks of the resting state networks. Figure from [3].

In this thesis, we formalize and extend the work of Atasoy et al. in a novel direction, both in terms of computational modeling and mathematical analysis. We here propose a more general framework based on the graph Laplacian, amenable to mathematical analysis and numerical simulations, which can be used to implement neural field models on the human connectome graph, as a powerful but relatively simple toolset to investigate the structure-function question. This approach may also be considered conceptually equivalent to implementing a whole-brain neural mass model on a connectome graph with high spatial resolution; but notably, the graph Laplacian allows explicit modeling of neural activity propagation, going beyond implicit "coupling" between regions. As an instructive example, we study a generalized, stochastic version of the Wilson-Cowan model employed in [3], where we include subcortical input and noise. Following in the line of many previous studies, for example [18, 44], we model resting-state brain dynamics as noise-induced, structured fluctuations about a steady state. Importantly, we note that the framework allows for more biophysically realistic models, whose qualities can then be put to the test by quantitative comparison with multimodal neuroimaging data. The core result of this work is therefore a framework for the translation continuous neural field models

to graphs, in particular the human connectome. Analytic results include linear stability analysis of the Wilson-Cowan model steady states, and most notably, predictions for the spatiotemporal power spectra and functional connectivity of noise-induced equilibrium fluctuations, which may be directly related to resting state brain activity. Numerical results include nonlinear simulations on a one-dimensional graph, and linearized simulations on the full human connectome graph, showing excellent agreement between the measured spatiotemporal spectra and the analytic predictions.

After this brief description of the context in which to place this work, we can now move on to describing the framework and results. In Section 2, we mention some concepts from neural field theory and define the continuous Wilson-Cowan neural field equations that we aim at translating on graphs; in Section 3, we discuss some notions from graph theory that are necessary to implement the continuous model on graphs; in Section 4, we give the full mathematical formulation of the graph stochastic Wilson-Cowan model and its linear stability analysis; in Section 5, we perform the spatiotemporal analysis of noise-induced fluctuations about the model steady states; in Section 6, we present the results of numerical simulations; and finally in Section 7 and 8, we discuss advantages, limitations and potential applications of this approach in relation to existing ones.

2. From Neural Fields to Neural Dynamics on Graphs

In this Section we briefly describe some basic concepts from neural field theory, and in particular the formulation of the continuous, stochastic Wilson-Cowan model that we aim at implementing on the human connectome graph.

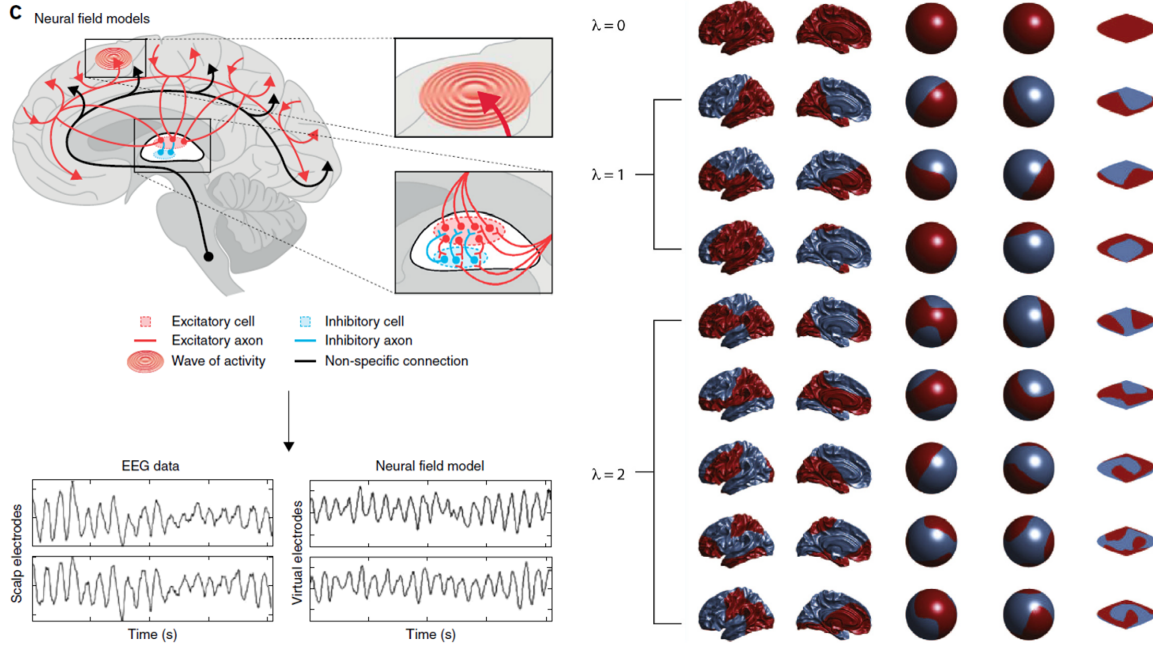


FIGURE 5. (a) Schematic representation of a continuous neural field model with a thalamic neural mass (top), shown to reproduce realistic EEG timecourses (bottom)(Figure adapted from [8]). (b) In [35], eigenmodes of a continuous neural field model on a spherical geometry are projected onto the cortex and a flat surface for visualization.

2.1. Neural Field Theory. — The goal of neural field theory is ultimately to identify the theoretical principles allowing functional brain activity and cognition [13], while avoiding some of the complications generated by the remarkable organizational complexity of the brain, particularly overspecialization and collection of disjointed facts. This is attempted by devising a simplified picture that should capture some of the relevant properties of the human brain, while also being mathematically and computationally tractable. The crucial assumption underlying neural field models is that on the scale of the full cortex, the properties of individual neurons may be aggregated into "mean field" population properties, and therefore neural tissue may be modeled as a continuum, while still bearing significant relation to the real system. This approximation has lead to significant advancement in the understanding of a wide range of neural phenomena: for example, explaining activity in neurological disorders and cognitive tasks (see [13] for an extensive review of the results of neural field theory, or [32, 35] and refs. therein for a brief overview). In most neural field models, continuous integrodifferential equations are used to mathematically model neural activity generation and propagation on a simplified geometry. This is often a flat, bidimensional sheet or the surface of a sphere, topologically equivalent to a brain hemisphere if the corpus callosum is disregarded⁽¹⁾. More sophisticated accounts also include one or multiple neural masses in the thalamus, driving the cortical neural field activity. Such models have been used to estimate neurophysiological parameters, reproduce cortical rhythms, and other neural phenomena such as anesthetic-induced effects [34, 36, 25]; in some cases, the dynamical properties of activity on the simplified geometry are related to the cortical dynamics by accounting post-hoc for the cortical folding with specific techniques [35].

⁽¹⁾The corpus callosum connects the left and right cerebral hemispheres, and enables communication between the hemispheres. It is the largest white matter structure in the human brain, consisting of 200-250 million axonal projections.

In this work, we suggest that it might be advantageous to implement integrodifferential neural field equations directly on the human connectome, in order to avoid some of the mathematical complexity and approximations of continuous neural fields; however, we are presented with the challenge of formulating such equations on a graph. Among the many available options, we focus on the Wilson-Cowan [14] model, because it is one of the most widely used and successful neural field models, and also by continuity with the work of Atasoy et al. However, it is important to remark that many variants of this model, or altogether different, more biophysically realistic neural field models, could be implemented and studied within this framework.

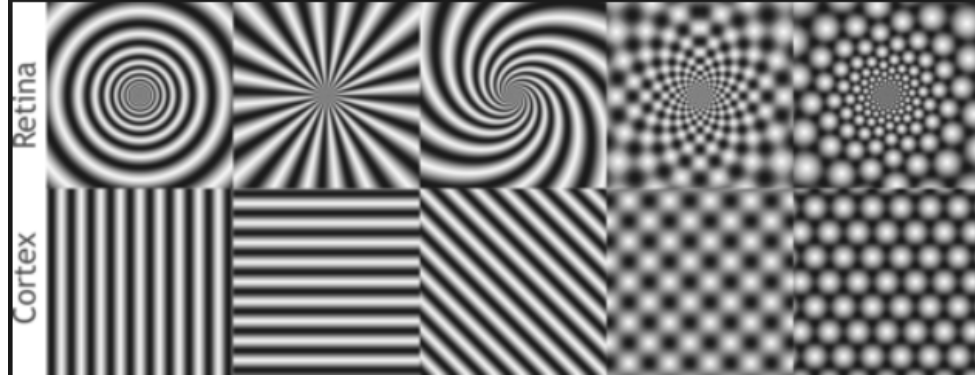


FIGURE 6. Regular patterns of neural activity in the visual cortex produced by a continuous 2D Wilson-Cowan model, and their corresponding retinotopic percept. Figure from [37].

2.2. The Wilson-Cowan Model. — The main goal of this work can be said to be that of implementing a stochastic Wilson-Cowan model on a high-resolution human connectome graph, and study it with a combination of numerical and analytic methods. The Wilson-Cowan model was originally developed in the late 1960s and early 1970s, following the considerations of Pitts and Wiener and building on early work by Beurle [7], who were among the first to advocate for a statistical approach to the study of neural dynamics on the cortex. That is, to focus on *population*-level properties (for example the fraction of neurons active at a given time in a local population) rather than studying networks of individual neurons, in order to formulate tractable cortical dynamics. As recounted by Jack Cowan himself in [13], he and Wilson intuited that an approach based on distinguishing Excitatory and Inhibitory populations might be useful to describe neural dynamics, by analogy with the famous Lotke-Volterra equations for predator-prey systems, which had been studied by Kerner in the early 1960s. This idea lead to the original formulation of the Wilson-Cowan model for spatially homogeneous [47] and inhomogeneous [48] populations, the latter of which contains spatial convolution integrals. Over the following decades, large amounts of applied and theoretical work have been carried out on the continuous Wilson-Cowan model from many different perspectives, including but not limited to spatiotemporal spectra, analysis of bifurcations, emergence of long-range correlations, and response to stimuli (See [14] and Chapter 2 of [13] for a review). Some important applications include modeling of pathological brain dynamics, in particular epilepsy [29], and even a theoretical explanation for the geometric patterns of hallucinations induced by flickering lights or experienced under the influences of psychedelic substances [21, 37]. This latter application lead in turn to a deeper understanding the visual cortex architecture [9] and of its evolutionary history [10]. Despite this body of work, the present is the first investigation of the spatiotemporal properties (power spectra and functional connectivity) of a graph Laplacian-based Wilson-Cowan model implemented on the human connectome.

2.2.1. Mathematical Formulation. — The continuous, stochastic Wilson-Cowan model takes the form of the following coupled integrodifferential equations:

$$(1) \quad \tau_E \partial_t E(x, t) = -d_E E(x, t) + S [\alpha_{EE}(G_{EE} * E)(x, t) - \alpha_{IE}(G_{IE} * I)(x, t) + P] + \sigma \xi_E(x, t),$$

$$(2) \quad \tau_I \partial_t I(x, t) = -d_I I(x, t) + S [\alpha_{EI}(G_{EI} * E)(x, t) - \alpha_{II}(G_{II} * I)(x, t) + Q] + \sigma \xi_I(x, t)$$

Symbol	Meaning
$E(x, t)$	Excitatory population activity.
$I(x, t)$	Inhibitory population activity.
τ_E, τ_I	Time constants.
d_E, d_I	Activity decay rates.
$S[x]$	Sigmoid $S[x] = 1/(1 + e^{-x})$.
$\alpha_{EE}, \alpha_{IE}, \alpha_{EI}, \alpha_{II}$	Strength of connectivity between populations.
$G_{EE}, G_{IE}, G_{EI}, G_{II}$	Convolution kernels.
P	Subcortical input to E populations.
Q	Subcortical input to I populations.
σ	Intensity of the intrinsic noise.
$\xi_E(x, t), \xi_I(x, t)$	Noise realization.

TABLE 1. Meaning of symbols in the continuous Wilson-Cowan Equations.

Where the symbol $*$ denotes a spatial convolution integral. In other words, this model posits the existence of two neuronal populations (Excitatory and Inhibitory) at each location in space. The temporal evolution of activity is given by a decay term with rate d_* , a sigmoid-mediated activation term containing the four combinations of population interactions ($E-E$, $I-E$, $E-I$, $I-I$) and the (constant) subcortical input terms P and Q , and finally the intrinsic noise $\sigma \xi_*(x, t)$. The coupling and propagation of activity among neuronal populations is modeled by the spatial convolution integrals with four, potentially different, kernels ($G_{EE}, G_{IE}, G_{EI}, G_{II}$). Note that this model formulation has some important differences with respect to that of Atasoy et al. in [3]. Namely, the addition of terms for subcortical input, the generalization to non-Gaussian convolution kernels, and crucially, the inclusion of *noise*, making the equations stochastic rather than deterministic, and allowing characterization of resting-state activity as noise-induced fluctuations about the model steady states in Section 5 (whereas [3] focused on limit-cycle oscillations, more akin to epileptic dynamics). The Wilson-Cowan model can produce both types of dynamics, depending on the choice of parameter set.

The "differential" aspect of the model refers to the time domain, because as usual the first temporal derivative is used to specify the model time-evolution. The implementation of the temporal derivative on graphs is relatively straightforward in this case, because the notion of time and of the first temporal derivative does not change in graph domain: time is still a continuous variable⁽²⁾. The "integral" aspect of the model refers to the spatial convolution integrals appearing in the equations, and is more challenging to translate on graphs, because we have to adapt the notion of spatial convolution integrals from continuous space to the discrete graph domain.

Spatial convolution integrals are used in this context to model activity coupling and propagation in space, with an appropriate kernel ("activity propagators"). The kernels models a spatially extended, connectivity weighting function between populations. The most commonly used kernels are familiar symmetric functions: for instance, Gaussian (as in [3]), double exponential, mexican-hat. We will show in Section 3 how it is possible to implement such spatial convolution integrals on a graph, by employing the graph Laplacian. More generally, we will also show that it is also possible to formulate time-evolution operators of ordinary differential equations on the graph (here, diffusion and the damped wave equation) which can be used in place of the spatial convolution integrals to model activity coupling and propagation on the connectome. These results further expand the repertoire of neural field models that can be implemented on the human connectome graph with the graph Laplacian framework.

⁽²⁾except of course in numerical simulations, where time discretization becomes necessary.

3. The Graph Laplacian Framework

In the first part of this section, loosely following [42], we define and describe the metric graph Laplacian operator, which is central for our implementation of neural field models on graphs, and its relation to continuous and finite difference Laplacians. We will then show how the graph Laplacian can be used to define the graph Fourier transform and implement spatial convolution integrals on graphs, such as those appearing in integrodifferential neural field equations, thereby circumventing the bidimensional-surface restriction of most continuous models, and the complexity of accounting post-hoc for cortical folding. Beyond spatial convolution integrals, we also show how to use the graph Laplacian to implement specific ordinary differential equations on the graph, modeling activity propagation dynamics.

3.1. The Metric Graph Laplacian. — In continuous n -dimensional Euclidean space, the Laplacian operator is given by

$$(3) \quad \Delta f(\mathbf{x}) = \sum_{i=1}^n \frac{\partial^2}{\partial x_i^2} f(x_i)$$

To define an equivalent of Δ on an undirected graph \mathcal{G} with N vertices, we start from the usual definitions of the graph adjacency matrix A and its diagonal degree matrix D :

$$(4) \quad A_{ij} = \begin{cases} 1 & \text{if } i \sim j \\ 0 & \text{otherwise} \end{cases} \quad D_{ii} = \sum_{j=1}^N A_{ij}$$

Let $f(\mathcal{G}) : \mathcal{G} \rightarrow \mathbb{R}^N$ be a real-valued function on the graph vertices. The directional derivative $\partial_j f_i$ at vertex i in the direction of vertex j can be defined as

$$(5) \quad \partial_j f_i = A_{ij} \frac{f_j - f_i}{d_{ij}},$$

where d_{ij} is the distance between vertices i and j . Note that by this definition, $\partial_j f_i = 0$ if vertex j is not connected to vertex i , and $\partial_i f_i = 0$ always. Furthermore, noting that $A_{ij}^2 = A_{ij}$, it follows directly that the second-order directional derivative $\partial_j^2 f_i$ is given by

$$(6) \quad \partial_j (\partial_j f_i) = \partial_j^2 f_i = A_{ij} \frac{f_i - f_j}{d_{ij}^2}.$$

The *metric graph Laplacian* operator can now be defined as⁽³⁾

$$(7) \quad \Delta_{\mathcal{G}} f_i = - \sum_{j=1}^N \partial_j^2 f_i,$$

We can write the operator in matrix form

$$(8) \quad \Delta_{\mathcal{G}} = \tilde{A} - \tilde{D},$$

where \tilde{A} and \tilde{D} are the distance-weighted adjacency and degree matrices, respectively

$$(9) \quad \tilde{A}_{ij} = A_{ij}/d_{ij}^2 \quad \tilde{D}_{ii} = \sum_{j=1}^N \tilde{A}_{ij},$$

Using the *metric* form of the graph Laplacian will be useful to preserve the connection with continuous

⁽³⁾One could also write $\nabla_{\mathcal{G}} = [\partial_1, \dots, \partial_N]$ for the "graph-gradient", and then define $\Delta_{\mathcal{G}} = -\nabla_{\mathcal{G}} \cdot \nabla_{\mathcal{G}}$. The minus sign arises to maintain the analogy with the continuous Laplacian.

neural fields. Δ_G is a metric graph invariant, and if distance weighting is omitted, the resulting (non metric) graph Laplacian is a topological invariant. The graph Laplacian (metric or not) is always a positive semi-definite matrix and hence has an orthogonal basis of eigenvectors. If the graph is the human structural connectome, the graph-Laplacian eigenvectors would be the "connectome harmonics" of [3]. Furthermore, the eigenvectors of the graph Laplacian define the Fourier transform on graphs, as we will discuss in Section 3.2.1.

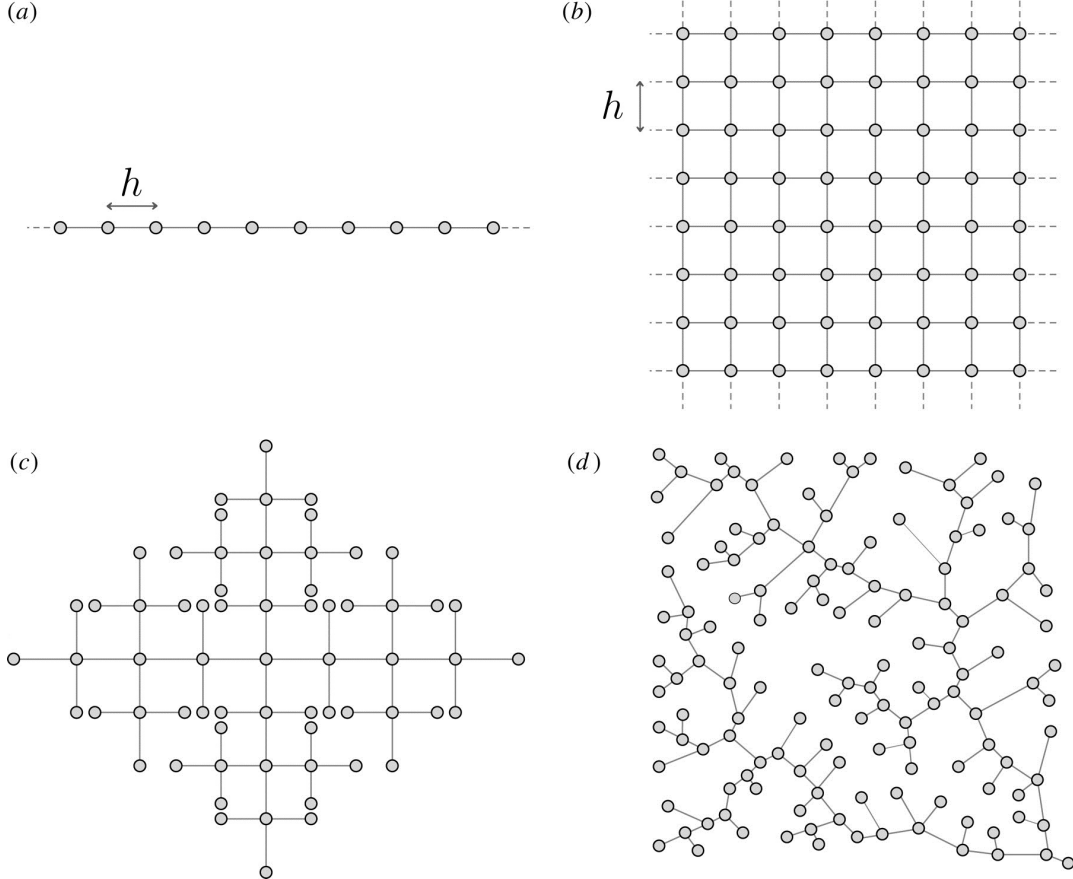


FIGURE 7. One-dimensional (a) and two-dimensional (b) regular graphs. (c) and (d) show examples of non-regular graphs in two-dimensional space. Figure adapted from [6].

3.1.1. Connection with Finite-Difference Laplacian. — An intuitive way to visualize the analogy between the graph Laplacian matrix and the continuous Laplacian operator is by examining the relation of the former with the discrete, finite-difference Laplacian operator. Consider a regular metric graph, that is a graph in which all nodes are connected only to their nearest neighbors (two in one dimension, four in two dimensions, six in three dimensions), and all edges have the same length h , thereby forming a chain in 1D, a square grid in 2D, and a cubic lattice in 3D. Such a regular graph corresponds to the spatial discretization used in finite-difference numerical simulations, and therefore in this case the graph and finite-differences Laplacians coincide. As an example, let us compute the graph Laplacian of a regular 1D graph with closed boundaries. We obtain the matrix:

$$(10) \quad \Delta_G = \tilde{A} - \tilde{D} = \frac{1}{h^2} \begin{bmatrix} -1 & 1 & & \cdots & 0 \\ 1 & -2 & 1 & & \vdots \\ & & \ddots & & \\ \vdots & & 1 & -2 & 1 \\ 0 & \cdots & & 1 & -1 \end{bmatrix}$$

which is indeed identical to the usual finite-difference 1D Laplacian matrix, such that for any function $f(\mathcal{G})$ on the vertices of the graph \mathcal{G} , we have

$$(11) \quad \Delta_{\mathcal{G}} f_i = \frac{f_{i+1} + f_{i-1} - 2f_i}{h^2}$$

In turn, the finite-difference Laplacian is well known to converge to the continuous Laplacian operator in the continuum limit. Periodic boundary conditions can be implemented much like in usual finite difference, by adding edges between the last and first nodes on each side of the regular graph.

It is important to remark at this point that the correspondence between metric graph Laplacian and continuous Laplacian operator holds exactly in the continuum limit *only* for regular graphs; for non-regular graphs, the analogy still holds, but as a more abstract property. For example, imagine a diffusion process taking place on an irregular graph such as those in Figure 7(c) or (d). Intuitively, a process taking place on an irregular graph will *not* be identical to a (continuous) diffusion process taking place in the Euclidean space that the graph is nonetheless embedded on, in this case a bidimensional surface. In particular, "non-local" effects (from the perspective of the continuous domain) due to the graph structure would appear, as we will see in practice in Section 3.3.1. Similarly, a Gaussian kernel formulated with the graph Laplacian formalism (Section 3.2) on non-regular graph domains such as those in Figure 7(c) or (d) will not be equivalent to a Gaussian distribution on the underlying continuous space, because it relies on the graph nodes and edges rather than the continuous space in which the graph is embedded; and should perhaps be called "graph-Gaussian", rather than simply Gaussian, to avoid confusion. This caveat actually constitutes a major strength of the graph Laplacian approach, because it allows us to directly model kernels or processes taking place on a graph nodes and edges, moving beyond regular discretization of continuous space.

Finally, we stress again the importance of using a metric graph-Laplacian by weighting the adjacency matrix according to the squared inverse of the Euclidean distance between each pair of (locally i.e. intracortically) connected nodes, in order to maintain a connection with continuous neural fields. The non-metric graph-Laplacian, such as the one used in [3] is a topological invariant of the graph, and therefore does not take into account the information contained in the distances between nodes. However, the distance metric for non-local connections need not be Euclidean and may be chosen according to the specifics of the case. For example, activity propagation on long-range (non-local) cortico-cortical connections in the human connectome may be better characterized by the distance along white matter fibers, rather than Euclidean distance.

3.2. Spatial Convolution Integrals on Graphs. — In Section 3.1 we have defined the metric graph Laplacian matrix, in connection with the finite-difference and the continuous Laplacian operators. We can use this analogy to implement spatial convolution integrals on graphs; and furthermore, we can also implement analogues of differential equations' time-evolution operators (e.g. the damped-wave equation) on graphs.

3.2.1. The Fourier Transform on Graphs. — The Fourier transform in continuous domains and the corresponding Fourier series are perhaps among the most commonly used tools in applied mathematics. They are both directly related to the continuous Laplacian operator, and indeed this relation is maintained between the graph Fourier transform and the graph Laplacian. The relation is given by the fact that the Fourier basis in continuous space is per definition also the eigenbasis of the continuous Laplacian operator. This means that taking the Fourier transform of a function is equivalent to projecting it onto the Laplacian eigenbasis (i.e. in both cases we obtain the coefficients of the Fourier decomposition). Similarly, it is possible to define the Fourier transform on the graph through the graph Laplacian eigenvectors. Note that the continuous Laplacian operator has infinite eigenfunctions with different spatial frequencies characterized by the wavenumber k ; whereas the graph-Laplacian only has as many eigenvectors as there are nodes in the graph, characterized by the corresponding graph Laplacian eigenvalues λ_k . For regular graphs, the eigenvectors of the graph Laplacian are identical (in the continuum limit) to the usual sinusoidal, harmonic functions that define the Fourier basis in continuous space. For non-regular graphs, the topology of the graph determines the exact

shape of the eigenvectors, but at least for the kind of graphs that we are concerned with (human connectomes) the eigenvectors can still be observed to follow sinusoidal patterns of increasing spatial frequency with increasing eigenvalues (See Figure 4).

Now, in order to formalize convolutions on graphs, let us start from the usual definition of the continuous Fourier transform, \mathcal{F} :

$$(12) \quad \mathcal{F}\{f(x)\} = \int_{-\infty}^{+\infty} e^{-ikx} f(x) dx = \hat{f}(k)$$

On the graph, diagonalizing the graph Laplacian we can write U for the matrix of column-eigenvectors, U^T for the matrix of row-eigenvectors, and Λ for the diagonal matrix of the graph Laplacian eigenvalues:

$$(13) \quad \Delta_{\mathcal{G}} = U \Lambda U^T, \quad \Lambda = \begin{bmatrix} \lambda_1 & & 0 \\ & \ddots & \\ 0 & & \lambda_N \end{bmatrix}$$

We can now define the Fourier transform of any function $f(\mathcal{G}) : \mathcal{G} \rightarrow \mathbb{R}^N$ on the graph simply as a multiplication from the left by the row-eigenvectors matrix U^T .

$$(14) \quad \mathcal{F} \equiv U^T, \quad U^T f(\mathcal{G}) = \beta^f(\lambda_k),$$

Note that the graph Fourier transform $\beta^f(\lambda_k)$ depends on the graph Laplacian eigenvalues rather than a fixed wavenumber; and therefore it also intrinsically depends on the structure of the specific graph \mathcal{G} . With this definition in place, it is possible to show that some important properties of the continuous Laplacian also hold for the graph Laplacian. In continuous space, the Fourier transform of the Laplacian of a function is equivalent to the Fourier transform of the original function, multiplied by the negative squared wavenumber. That is:

$$(15) \quad \mathcal{F}\{\Delta f(\mathbf{x})\} = -k^2 \hat{f}(k)$$

On the graph, a similar relation holds. We have defined the Fourier transform as a matrix multiplication from the left by the graph Laplacian row eigenvectors in Eqn. 14; and diagonalizing the graph Laplacian as per Eqn. 13, we have:

$$(16) \quad U^T \{\Delta_{\mathcal{G}} f(\mathcal{G})\} = U^T \{U \Lambda U^T f(\mathcal{G})\} = \Lambda \beta^f(\lambda_k) = \lambda_k \circ \beta^f(\lambda_k)$$

In the last step, we have simply written the product of the diagonal matrix of eigenvalues Λ with the graph Fourier transform $\beta^f(\lambda_k)$ as a pointwise (Hadamard) product. Note that the negative squared wavenumber $-k^2$ in Eqn. 15, is substituted in its graph-analogue Eqn. 16 by the k^{th} graph Laplacian eigenvalue λ_k . The analogy $-k^2 \rightarrow \lambda_k$ will be important for the translation of convolution integrals on graphs.

3.2.2. The Convolution Theorem on Graphs. — The convolution theorem states that a convolution integral (in continuous space) becomes a pointwise product in the corresponding Fourier space. In other words, the continuous Fourier transform of a convolution with kernel $g(x)$ of an arbitrary function $f(x)$ is

$$(17) \quad \mathcal{F}\{(g * f)(x)\} = \hat{f}(k) \hat{g}(k)$$

We can use the theorem to obtain an equivalent definition of a convolution integral as a composition of operators applied to the function to be convolved, $f(x)$. This would be 1) Fourier transform $f(x)$; 2) Multiply pointwise (in k -space) by the Fourier transform of the kernel $\hat{g}(k)$; 3) Inverse Fourier

transform. In other words, we can define a convolution integral as:

$$(18) \quad (g * f)(x) = \mathcal{F}^{-1}\{\hat{g}(k)\hat{f}(k)\}$$

This is useful because we have already obtained translations on the graph for each individual operator in this composition (Fourier transform, pointwise product, inverse Fourier transform). Therefore, we can use it to obtain a translation of the convolution integral as a product of matrix operators on the graph. Recall that the inverse Fourier transform \mathcal{F}^{-1} is defined on the graph by the column eigenvector matrix U . We can then define an analogue of the convolution integral on graphs as

$$(19) \quad (g * f)(\mathcal{G}) = U\{\beta^g(\lambda_k) \circ \beta^f(\lambda_k)\} = U\{\beta^g(\Lambda)U^T f(\mathcal{G})\} = \beta^g(\Delta_{\mathcal{G}})f(\mathcal{G})$$

We have thus obtained a representation of the convolution integral on graphs⁽⁴⁾ as an operator $\beta^g(\Delta_{\mathcal{G}})$, matrix-function of the graph Laplacian, acting on the function to be convolved $f(\mathcal{G})$. It is now almost trivial to show that this definition is such that the convolution theorem is respected on graphs:

$$(20) \quad U^T\{(g * f)(\mathcal{G})\} = U^T\beta^g(\Delta_{\mathcal{G}})f(\mathcal{G}) = U^TU\beta^g(\Lambda)U^Tf(\mathcal{G}) = \beta^g(\lambda_k) \circ \beta^f(\lambda_k)$$

Note how in the definition of convolutions on graphs, Eqn. 19, the Fourier transform of the kernel also determines its convolution operator $\beta^g(\Delta_{\mathcal{G}})$. Combining this remark with the previous $-k^2 \rightarrow \lambda_k$, we can directly formulate convolution matrix operators on graphs. In other words, for a kernel with continuous Fourier transform $\hat{g}(k)$:

$$(21) \quad \beta^g(\Delta_{\mathcal{G}}) \equiv \hat{g}\left(\sqrt{-\Delta_{\mathcal{G}}}\right) = U\hat{g}\left(\sqrt{-\Lambda}\right)U^T = U \begin{bmatrix} \hat{g}(\sqrt{-\lambda_1}) & & 0 \\ & \ddots & \\ 0 & & \hat{g}(\sqrt{-\lambda_N}) \end{bmatrix} U^T$$

Eqn. 21 allows us to practically define the convolution operator on graphs, with the knowledge of the diagonalized graph Laplacian, and the continuous Fourier transform of the kernel at hand. This is an important result for the purposes of the current work, because it allows us to translate on the graph neural field models where such convolution integrals may arise. We note that the analogy $-k^2 \rightarrow \lambda_k$ restricts the application to even and real kernels.

Kernel	Continuous FT $[\hat{g}(k)]$	Graph Convolution Operator $[\beta^g(\Delta_{\mathcal{G}})]$
Gaussian	$2\sqrt{\pi t}e^{-tk^2}$	$U2\sqrt{\pi t}e^{t\Lambda}U^T$
Double Exponential	$\frac{2t}{t^2+k^2}$	$U\frac{2t}{t^2-\Lambda}U^T$
Mexican Hat	$4t\sqrt{\pi t}k^2e^{-tk^2}$	$-U4t\sqrt{\pi t}\Lambda e^{t\Lambda}U^T$
Pyramid	$tsinc^2\left(\frac{tk}{2\pi}\right)$	$Utsinc^2\left(\frac{t\sqrt{-\Lambda}}{2\pi}\right)U^T$
Rectangular	$tsinc\left(\frac{tk}{2\pi}\right)$	$Utsinc\left(\frac{t\sqrt{-\Lambda}}{2\pi}\right)U^T$

TABLE 2. Formulation of convolution operators on graphs, with $sinc(x) = \frac{\sin(\pi x)}{\pi x}$. We have included prefactors in this table s.t. all the kernels have unitary height.

⁽⁴⁾Note that an equivalent result appeared previously in [38].

3.2.3. Examples of Kernels on Graphs. — In Table 2, we show some examples of convolution operators on graphs computed according to Eqn. 21. For simplicity, we only implement convolution kernels with one parameter, denoted t , but it is possible to devise more complicated kernels with multiple independent parameters⁽⁵⁾.

To test the correctness of this formulation, we can apply the graph convolution operators to a Dirac delta function, or impulse function. That is, a function that is zero everywhere except for a specific location (in our case, a specific node on the graph), and integrates (sums up) to one over the whole domain. If the formulation is correct, on a *regular* graph the result of this operation should have exactly the familiar shape of the chosen kernel, centered at the location of the impulse function, as is the case for continuous convolution integrals. We implement this test numerically on a one-dimensional regular graph. The results, reported in Figure 8, confirm the validity of this approach.

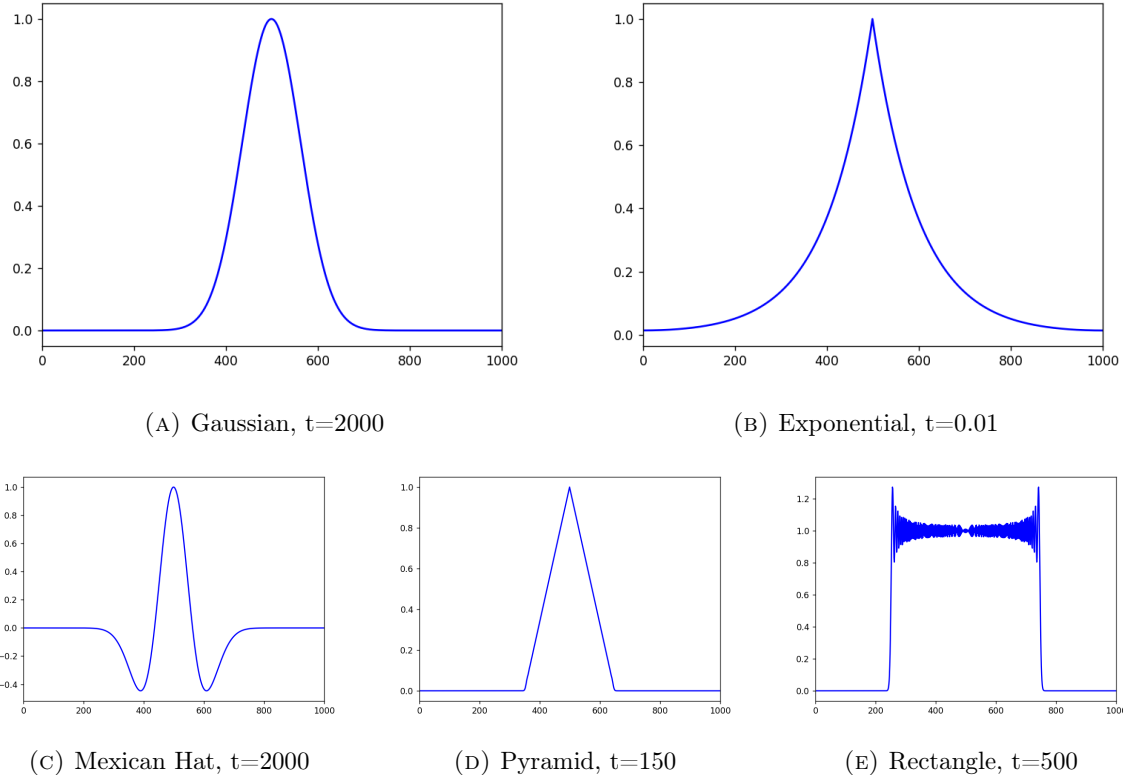


FIGURE 8. Results from applying the convolution operators defined in Table 2 to a unitary impulse function, centered on the mid-node of a 1-dimensional regular graph with spacing $h = 1$. Note that the convolution operator of the rectangular kernel in Figure 8e shows a significant amount of the *Gibbs phenomenon* [24], a known feature of finite Fourier series of functions with jump discontinuities. Solutions to this problem have been offered [23], but they are beyond the scope of the current work. Kernels with jump discontinuities should therefore be avoided in the formulation of neural field models with the graph Laplacian approach, for the time being.

⁽⁵⁾In fact, the Wilson-Cowan model which is the main focus of this study includes an "extra" independent parameter α_{**} for each of the four kernels appearing in the equations, representing the strength of coupling between population.

3.3. Time Evolution Operators on Graphs. — Having obtained a translation of spatial convolution integrals, we can also attempt to translate the time-evolution operators of ordinary differential equations on the graph. We can then use these operators to model activity propagation within the neural field model of choice. This further expand the repertoire of neural field models that can be implemented and studied on the human connectome with the graph Laplacian formalism.

3.3.1. The Diffusion Equation on Graphs. — The continuous diffusion equation (Eqn. 22, left side) is a particularly simple case, because its solution is just a convolution of the initial condition with a Gaussian kernel. We have therefore already derived its time-evolution operator on the graph in the previous section, as the Gaussian convolution operator (the matrix-exponential of the graph Laplacian, see Table 2). In fact, the diffusion equation on graphs (Eqn. 22, right side) has been previously studied, for example in the context of signal processing on graphs [41]. Nonetheless, it is instructive to briefly discuss and compare the two, before moving on to the slightly more complicated damped-wave equation. Note that in the continuous diffusion equation, $f(\mathbf{x}, t)$ is a scalar quantity evaluated at the position $\mathbf{x} \in \mathbb{R}^n$ and the Laplacian is an operator on the function space; whereas in the graph case, $f(\mathcal{G}, t)$ is the vector containing the value of the function f at each node in the graph, and $\Delta_{\mathcal{G}}$ is a constant matrix operator.

$$(22) \quad \frac{\partial f(\mathbf{x}, t)}{\partial t} = \Delta f(\mathbf{x}, t), \quad \frac{df(\mathcal{G}, t)}{dt} = \Delta_{\mathcal{G}} f(\mathcal{G}, t)$$

In continuous space, the solution to the diffusion equation with an arbitrary initial condition can be found by applying the convolution theorem and Green's function method. The solution at time t takes the form of an convolution with a Gaussian kernel of standard deviation $\sqrt{2t}$. On the other hand, a solution for the diffusion equation on the graph can be found simply by noting that the graph Laplacian is a constant matrix. Therefore we can write the two solutions, with arbitrary initial conditions, side by side:

$$(23) \quad f(\mathbf{x}, t) = \frac{1}{(4\pi t)^{\frac{n}{2}}} \int_{\mathbb{R}^n} e^{-\frac{|\mathbf{x}-\mathbf{y}|^2}{4t}} f(\mathbf{y}, 0) d\mathbf{y}, \quad f(\mathcal{G}, t) = e^{t\Delta_{\mathcal{G}}} f(\mathcal{G}, 0)$$

where, indeed, $e^{t\Delta_{\mathcal{G}}} = U e^{t\Lambda} U^T$ is the same matrix exponential operator (up to a prefactor) that we have previously found when translating the Gaussian convolution integral to the graph, thereby confirming by a different route the validity of the procedure presented in Section 3.2. Note that the *absence* of the prefactor is the correct formulation for a physical (conservative) diffusion process. In the context of the diffusion equation, t is the actual time variable, rather than simply a free parameter of the kernel.

Furthermore, it is interesting to remark that the usual forward-time finite-difference numerical scheme is simply equivalent to a first-order approximation of the graph Laplacian matrix exponential (which indeed represents the exact solution). Applying the forward-time approximation of the temporal derivative to the graph diffusion equation we have:

$$\begin{aligned} \frac{f(\mathcal{G}, \delta t) - f(\mathcal{G}, 0)}{\delta t} &= \Delta_{\mathcal{G}} f(\mathcal{G}, 0), & f(\mathcal{G}, \delta t) &= (\mathbb{1} + \delta t \Delta_{\mathcal{G}}) f(\mathcal{G}, 0) \\ f(\mathcal{G}, t) &= (\mathbb{1} + \delta t \Delta_{\mathcal{G}})^{\frac{t}{\delta t}} f(\mathcal{G}, 0), & \lim_{\delta t \rightarrow 0} (\mathbb{1} + \delta t \Delta_{\mathcal{G}})^{\frac{t}{\delta t}} &= e^{t\Delta_{\mathcal{G}}} \end{aligned}$$

Which is again the matrix exponential of the graph Laplacian. The linear approximation of the graph Laplacian matrix exponential is of practical utility. It was in fact employed by Atasoy et al. in [3] to simplify numerical simulations of the Wilson-Cowan model on the full human connectome, because indeed the matrix exponential of the connectome graph Laplacian is a very large and dense matrix.

To test the correctness of this formulation, we can simulate the time-evolution of a diffusion process on a regular 1-dimensional graph with closed boundaries. It is sufficient to choose a small value of $t \rightarrow \delta t$, and iteratively apply the matrix-exponential of the graph Laplacian $e^{\delta t \Delta_{\mathcal{G}}}$ starting from some arbitrary initial condition. The timecourse for a Dirac delta initial condition of height=10

is shown in Figure 9.

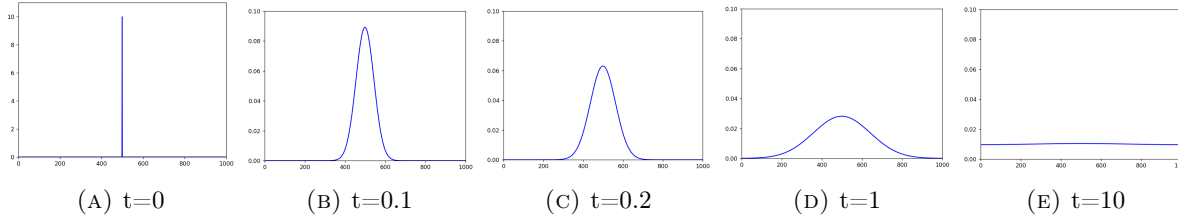


FIGURE 9. Time-evolution of diffusion on a regular 1D graph by iterative application of the graph Laplacian matrix exponential, with $\delta t = 0.01$ (indicating by t the total time elapsed) and internode spacing $h = 0.01$. Note that, as expected for a conservative process, the asymptotic solution is a constant (0.01) which integrates over the whole domain (comprising of 1000 nodes) to the same value of the initial condition (10).

Beyond regular graphs and the continuum analogy, it is important to remark that the real utility of the graph Laplacian formalism is the possibility of modeling processes taking place on the nodes and edges of arbitrary non-regular graphs, such as the human connectome, which is indeed what we are interested in here. To clarify this concept, we can add some non-local edges ("synapses") to the 1-dimensional regular graph, connecting the nodes at positions 500-520 to those at positions 700-720. We then re-calculate the metric graph Laplacian and its matrix exponential, and repeat the previous simulation of diffusion, but this time in the different context of an irregular, non-locally connected graph. As expected, the substance ("neural activity") diffuses non-locally (but still in a distance-based⁽⁶⁾ manner, thanks to the metric graph Laplacian) through the new edges, leading to a different time-evolution from diffusion on a regular graph. The timecourse of diffusion on a non-regular graph, with the same Dirac delta initial condition is shown in Figure 10.

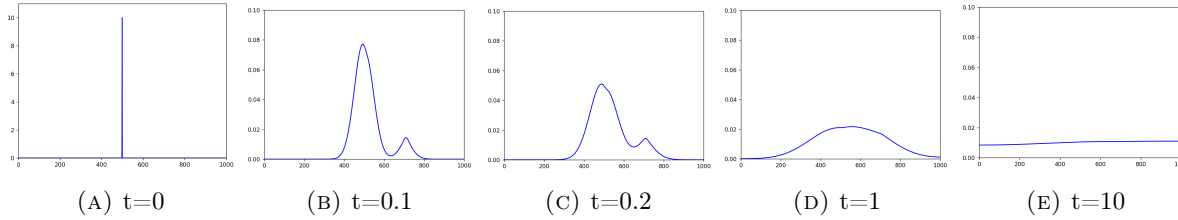


FIGURE 10. Time-evolution of diffusion on a non-regular 1D graph with metric edges from nodes 500-520 to nodes 700-720, $\delta t = 0.01$ (indicating by t the total time elapsed) and internode spacing $h = 0.01$. Note the emergence of a second "bump", due to the non-local edges. Note also that the asymptotic behavior is identical: both diffusion processes are conservative, therefore regardless of non-local edges, they approach the same constant solution as $t \rightarrow \infty$, as expected.

⁽⁶⁾Note that here we used the Euclidean distance between nodes for both local and non-local edges. Alternatively, we could have used a non-Euclidean metric for the non-local edges, for example modeling a longer path distance of diffusion, much like in the case of white matter fibers.

3.3.2. The Damped Wave Equation on Graphs. — Let us now consider the damped-wave equation on graphs, with scalar parameters a and b

$$(24) \quad a \frac{d^2 f(\mathcal{G}, t)}{dt^2} + b \frac{df(\mathcal{G}, t)}{dt} - \Delta_{\mathcal{G}} f(\mathcal{G}, t) = 0$$

Take the graph-Fourier transform by multiplying from the left by U^T , and writing $U^T f(\mathcal{G}) = \beta(\lambda_k)$, the system is diagonalized

$$(25) \quad a \ddot{\beta}(\lambda_k, t) + b \dot{\beta}(\lambda_k, t) - \Lambda \beta(\lambda_k, t) = 0$$

In other words, in the graph Fourier domain we have N decoupled scalar differential equations, describing the independent time-evolution of each graph Laplacian eigenmode

$$(26) \quad a \ddot{\beta}_k(t) + b \dot{\beta}_k(t) - \lambda_k \beta_k(t) = 0$$

These equations have exact solutions:

$$(27) \quad \beta_k(t) = \frac{r_1 e^{r_2 t} - r_2 e^{r_1 t}}{r_1 - r_2} \beta_k(0) + \frac{e^{r_1 t} - e^{r_2 t}}{r_1 - r_2} \dot{\beta}_k(0), \quad r_{1,2} = \frac{-b \pm \sqrt{b^2 + 4a\lambda_k}}{2a}$$

We can now use this expression to formulate a time-evolution operator for the damped-wave equation on the graph, simply by applying the inverse graph Fourier transform U

$$(28) \quad f(\mathcal{G}, t) = U \frac{r_1 e^{r_2 t} - r_2 e^{r_1 t}}{r_1 - r_2} U^T f(\mathcal{G}, 0) + U \frac{e^{r_1 t} - e^{r_2 t}}{r_1 - r_2} U^T \dot{f}(\mathcal{G}, 0), \quad r_{1,2} = \frac{-b \pm \sqrt{b^2 + 4a\Lambda}}{2a}$$

or, more compactly

$$(29) \quad f(\mathcal{G}, t) = \beta^{DW}(\Delta_{\mathcal{G}}) f(\mathcal{G}, 0) + \beta^{DW1}(\Delta_{\mathcal{G}}) \dot{f}(\mathcal{G}, 0)$$

Note that the damped-wave equation is second order in time, and as such requires two initial conditions to be specified. In order to test the correctness of this formulation, we can attempt to simulate the time-evolution of a damped wave equation on a regular 1D-graph, independently of the Wilson-Cowan model. This can be done by choosing a small $t \rightarrow \delta t$ and iteratively applying the operator, much like we did for the diffusion equation. The second initial condition $\dot{\beta}_k(0)$ is specified at each iteration of the operator as the usual finite-difference approximation of the first temporal derivative, that is difference in the function value at two consecutive timepoints, divided by δt .

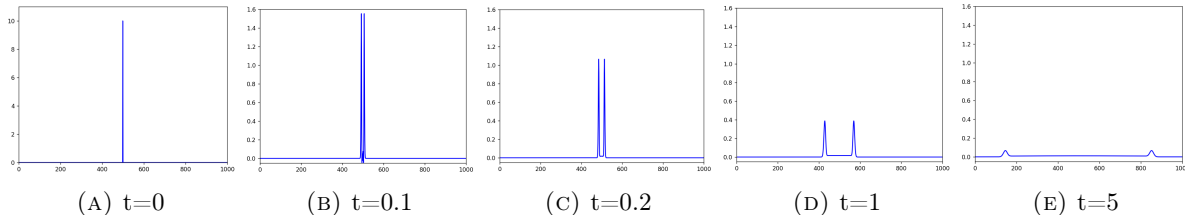


FIGURE 11. Time-evolution of the damped-wave equation on a regular 1D graph, with $\delta t = 0.01$ (indicating by t the total time elapsed), internode spacing $h = 0.01$, and the scalar parameters $a = b = 1$.

For the purposes of modeling activity propagation in neural field models, we can simply set the time-derivative initial condition $\dot{f}(\mathcal{G}, 0)$ to be zero, since the time variable t is treated as a free parameter of

the kernel, rather than an actual "time". We thus obtain a suitable expression for the time-evolution operator of the damped wave equation ($\beta^{DW}(\Delta_{\mathcal{G}})$), as a matrix-function of the graph Laplacian, similarly to those of Table 2:

$$(30) \quad \beta^{DW}(\Delta_{\mathcal{G}}) = U \frac{r_1 e^{r_2 t} - r_2 e^{r_1 t}}{r_1 - r_2} U^T, \quad r_{1,2} = \frac{-b \pm \sqrt{b^2 + 4a\Lambda}}{2a}$$

4. The Wilson-Cowan Model on Graphs

4.1. Mathematical Formulation. — We now have all the tools to implement a generalized, stochastic version Wilson-Cowan model on the human connectome (or any other metric graph of interest), with the convolution integrals or time-evolution operators that we derived in Section 3 represented as matrix-functions of the graph-Laplacian $\beta_{**}(\Delta_G)$ ("activity propagators"). A different propagator can be specified for each of the four interaction types EE, IE, EI, II . The model is formulated as a set of $2N$ coupled nonlinear differential equations, tracking the combined evolution of excitatory and inhibitory activity at each node in the graph:

$$(31) \quad \tau_E \dot{\mathbf{E}}(\mathcal{G}, t) = -d_E \mathbf{E}(\mathcal{G}, t) + S[\alpha_{EE}\beta_{EE}(\Delta_G)\mathbf{E}(\mathcal{G}, t) - \alpha_{IE}\beta_{IE}(\Delta_G)\mathbf{I}(\mathcal{G}, t) + P] + \sigma \xi_E(\mathcal{G}, t)$$

$$(32) \quad \tau_I \dot{\mathbf{I}}(\mathcal{G}, t) = -d_I \mathbf{I}(\mathcal{G}, t) + S[\alpha_{EI}\beta_{EI}(\Delta_G)\mathbf{E}(\mathcal{G}, t) - \alpha_{II}\beta_{II}(\Delta_G)\mathbf{I}(\mathcal{G}, t) + Q] + \sigma \xi_I(\mathcal{G}, t)$$

Symbol	Meaning
$\mathbf{E}(\mathcal{G}, t)$	Excitatory populations activity.
$\mathbf{I}(\mathcal{G}, t)$	Inhibitory populations activity.
τ_E, τ_I	Time constants.
d_E, d_I	Decay rate.
$S[x]$	Sigmoid $S[x] = 1/(1 + e^{-x})$.
$\alpha_{EE}, \alpha_{IE}, \alpha_{EI}, \alpha_{II}$	Strength of connectivities between populations.
$\beta_{EE}(\Delta_G), \beta_{IE}(\Delta_G), \beta_{EI}(\Delta_G), \beta_{II}(\Delta_G)$	Activity propagators (convolutions, ODEs)
P	Subcortical input to \mathbf{E} populations.
Q	Subcortical input to \mathbf{I} populations.
σ	Intensity of the intrinsic noise ξ_*
$\xi_E(\mathcal{G}, t), \xi_I(\mathcal{G}, t)$	Noise realization.

TABLE 3. Meaning of symbols in the Wilson-Cowan Equations.

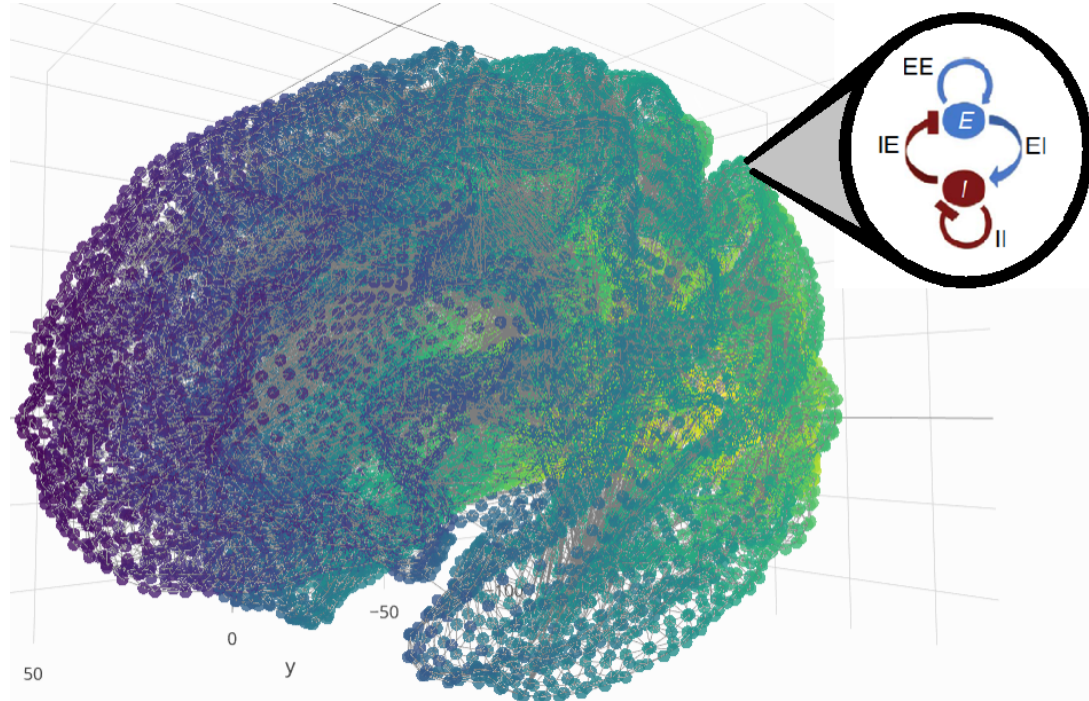


FIGURE 12. Simplified representation of the Wilson-Cowan model and the connectome that we use in this study. The thin grey lines represent structural connections (graph edges).

As an example, we study the Wilson-Cowan model with Gaussian-kernel propagators of different widths, that is: $\beta_{**}(\Delta_G) = U e^{t_{**}\Lambda} U^T$. Note that we could also specify altogether different kernels for each of the four propagators between **E/I** populations; and note also that for compactness we absorb the kernel prefactors of Table 2 in the connectivity parameters α_{**} . Equivalently, we might say that the chosen propagators are the time-evolution operators of the diffusion equation on the graph (Eqns. 22-23).

$$(33) \quad \tau_E \dot{\mathbf{E}}(\mathcal{G}, t) = -d_E \mathbf{E}(\mathcal{G}, t) + S[\alpha_{EE} U e^{t_{EE}\Lambda} U^T \mathbf{E}(\mathcal{G}, t) - \alpha_{IE} U e^{t_{IE}\Lambda} U^T \mathbf{I}(\mathcal{G}, t) + P] + \sigma \xi_E(\mathcal{G}, t)$$

$$(34) \quad \tau_I \dot{\mathbf{I}}(\mathcal{G}, t) = -d_I \mathbf{I}(\mathcal{G}, t) + S[\alpha_{EI} U e^{t_{EI}\Lambda} U^T \mathbf{E}(\mathcal{G}, t) - \alpha_{II} U e^{t_{II}\Lambda} U^T \mathbf{I}(\mathcal{G}, t) + Q] + \sigma \xi_I(\mathcal{G}, t)$$

The parameter set of choice for all explicit numerical and analytic results, unless otherwise stated, is reported in Table 4. This parameter set was determined by qualitative comparison with fMRI data (see Section 5.3 for details).

Parameter	Value
τ_E	4.95
τ_I	4.48
d_E	14.37
d_I	1.09
α_{EE}	115.36
α_{IE}	180.82
α_{EI}	189.77
α_{II}	210.31
t_{EE}	35.08
t_{IE}	3.77
t_{EI}	$6.7 \cdot 10^{-4}$
t_{II}	$5.091 \cdot 10^3$
P	5.37
Q	5.31
σ	10^{-5}

TABLE 4. Parameter set choice for explicit analysis and numerical simulations, based on a qualitative comparison with empirical data (see Section 5.3). We use unit-less parameters for simplicity, but this in turn implies that their values do not refer directly to any specific biophysical parameter.

4.1.1. Connection with Neural Mass Models. — It is interesting to remark at this point an intuitive connection of this approach to neural *mass* models. If we consider the current Wilson-Cowan model with all Gaussian kernel parameters $t_{**} = 0$, we obtain a model in which all nodes are disconnected, and each behaves like an independent Wilson-Cowan system. In neural mass models, a matrix of coupling strengths, often inferred by group-averaged white matter tracts, is often used to create a correlated network of such nodes and study properties such as synchronization. Here instead, thanks to the graph Laplacian formalism, we can attempt to explicitly model the propagation of activity on the connectome, moving beyond the more implicit coupling concept. Therefore, it is possible to conceptualize this approach either as the translation of a neural field model on a graph, but also as a neural mass model in which activity propagation is explicitly modeled.

4.2. Linear Stability Analysis. — For all explicit analysis and numerical simulations, we use the *space-independent* (scalar) parameter set of Table 4 (i.e. the parameters are identical for each node on the connectome). However, it is possible to generalize at least some parts of the analysis to non-constant parameters. For generality and compactness of notation, let us define a new column vector $\mathbf{z}(t)$ as the concatenation of $\mathbf{E}(t)$ and $\mathbf{I}(t)$; We express \mathbf{d} for the diagonal matrix containing the damping parameters d_E and d_I and $\boldsymbol{\tau}$ for the matrix containing the timescale parameters τ_E and τ_I . The matrix K contains the four (arbitrary) propagators, \mathbf{X} is the concatenated vector encoding subcortical inputs P and Q , and $\boldsymbol{\xi}$ contains the concatenated noise realizations for all populations. We

can now write the original system, with a single equation, potentially allowing for space-dependent parameters:

$$(35) \quad \tau \dot{\mathbf{z}}(t) = -\mathbf{d}\mathbf{z}(t) + \mathbf{S}[\mathbf{K}\mathbf{z}(t) + \mathbf{X}] + \sigma \xi$$

The steady-state \mathbf{z}^* of the above model can be obtained in the absence of noise by setting the time-derivative to zero and solving the resulting steady state (matrix) equation:

$$(36) \quad \mathbf{S}[\mathbf{K}\mathbf{z}^* + \mathbf{X}] = \mathbf{d}\mathbf{z}^*$$

Solving this equation efficiently is necessary for linear stability analysis, since the Jacobian of the linearized system for any given set of parameter depends also on the steady state values. However, this equation does not have an analytic, exact, closed form solution (in fact, it doesn't even necessarily have a solution. The sigmoid function is bound between -1 and 1, but $\mathbf{d}\mathbf{z}^*$ is not). Furthermore, in the context of a whole-brain model, the equation is very high dimensional (twice the number of nodes, so ~ 40000 in our case), making a brute-force numerical approach, which would have to be repeated for each parameter set, computationally inefficient.

4.2.1. Solutions to the Steady State Equations. — However, the problem simplifies if we restrict our analysis to *spatially homogeneous* steady states (i.e. \mathbf{E}^* and \mathbf{I}^* are two constants, not necessarily the same), we can take advantage of the fact that action of activity propagators on a constant state is the same as the identity (intuitively, for example, the convolution of a Gaussian kernel with a constant function returns the same constant). Therefore, assuming a spatially homogeneous steady state, the equation simplifies to

$$(37) \quad \mathbf{S}[\alpha \mathbf{z}^* + \mathbf{X}] = \mathbf{d}\mathbf{z}^* \quad \begin{bmatrix} \alpha_{EE} & -\alpha_{IE} \\ \alpha_{EI} & -\alpha_{II} \end{bmatrix} = \alpha$$

Where α_{**} and \mathbf{d} matrices are positive diagonal (not necessarily constant) matrices of size $2N \times 2N$ containing the connectivity strength and decay parameters for each node; and as before \mathbf{X} is the concatenated vector encoding subcortical inputs P and Q . This matrix equation is simpler, but still very high dimensional, and not necessarily solvable.

However, assuming that all the model parameters are *space-independent*, each diagonal matrix α_{**} is constant and can be substituted by their scalar value. More precisely, the α_{**} and \mathbf{d} matrices and the \mathbf{X} vector can be rewritten as Kronecker products involving the identity matrix of size N and the vector of 1s of the same size, respectively. In this case, to find the steady state we only have to numerically solve the following 2-dimensional system, rather than the original $2N$ -dimensional matrix equation 36:

$$(38) \quad \frac{1}{1 + \exp(\alpha_{IE}I^* - \alpha_{EE}E^* - P)} = d_E E^*$$

$$(39) \quad \frac{1}{1 + \exp(\alpha_{II}I^* - \alpha_{EI}E^* - Q)} = d_I I^*$$

The steady state(s) of the model are given by the real and positive solutions of this system of equations, which can be quickly obtained numerically. Once a steady state solution is obtained, its stability can be studied through the Jacobian eigenvalues; in turn, both the existence and stability of the steady state solution have to be checked with numerical simulations. For the parameter set of Table 4, the equations are found to have a single suitable solution, and therefore the model has only one steady state, $E^* = 0.0076$ and $I^* = 0.0461$.

It is also possible to consider one of the simplest special cases, where there is no external input and $\alpha_{**} = 1$. In this case, it is possible to obtain exact closed-form analytic solutions for E^* and I^* ,

but these expressions are more complicated than they are insightful. However, if we further assume $d_I = d_E$ we can obtain the extremely simple solutions $I^* = E^* = 1/2d_E = 1/2d_I$. And we can note that this is still a leading order approximation to the true solution if $d_I \approx d_E$. We might speculate that this is why this approximation was used as the steady state solution in [3] (Supplementary Materials, page 15), although no formal justification is offered there. In any case, this simple solution should not be considered an exact or even reliable to the true solution(s) in the vast majority of cases.

4.2.2. General Wilson-Cowan Jacobian. — After the solutions of the steady state equation for a given parameter set (space-independent or not) have been obtained, we can determine its stability by studying the Jacobian eigenspectrum. Going back to the linearized model in the standard form:

$$(40) \quad \dot{\mathbf{z}}(t) = -\boldsymbol{\tau}^{-1}\mathbf{d}\mathbf{z}(t) + \boldsymbol{\tau}^{-1}\mathbf{S}[K\mathbf{z}(t) + \mathbf{X}] = F(\mathbf{z}) \approx F(\mathbf{z}^*) + \left. \frac{\partial F(\mathbf{z})}{\partial \mathbf{z}} \right|_{\mathbf{z}^*} \delta\mathbf{z}$$

With $F(\mathbf{z}^*) = 0$, and defining a small perturbation about the steady state $\delta\mathbf{z} = (\mathbf{z} - \mathbf{z}^*)$. We can study the evolution of the perturbation about a steady state by looking at the Jacobian of the linearized system:

$$(41) \quad J(\mathbf{z}^*) = \left. \frac{\partial F(\mathbf{z})}{\partial \mathbf{z}} \right|_{\mathbf{z}^*} = -\boldsymbol{\tau}^{-1}\mathbf{d} + \text{Diag}(\boldsymbol{\tau}^{-1}\mathbf{S}'[K\mathbf{z}^* + \mathbf{X}]) K$$

By applying the property of the sigmoid derivative $S'(x) = S(x)(1 - S(x))$; the steady state equation $\mathbf{S}[K\mathbf{z}^* + \mathbf{X}] = \mathbf{d}\mathbf{z}^*$; and finally denoting with \circ the Hadamard product we can note that

$$\text{Diag}(\boldsymbol{\tau}^{-1}\mathbf{S}'[K\mathbf{z}^* + \mathbf{X}]) = \text{Diag}(\boldsymbol{\tau}^{-1}\mathbf{S}[K\mathbf{z}^* + \mathbf{X}] \circ (\mathbf{1} - \mathbf{S}[K\mathbf{z}^* + \mathbf{X}])) = \text{Diag}(\boldsymbol{\tau}^{-1}\mathbf{d}\mathbf{z}^* \circ (\mathbf{1} - \mathbf{d}\mathbf{z}^*))$$

We can now write the Jacobian in a very compact form, remarking that $\boldsymbol{\tau}^{-1}\mathbf{d}$ is a (potentially non-constant) diagonal matrix depending on the model parameters. K is as usual a dense matrix containing the graph Laplacian propagators, and therefore encapsulates most of the complexity of the Jacobian

$$(42) \quad J(\mathbf{z}^*) = -\boldsymbol{\tau}^{-1}\mathbf{d} + \text{Diag}(\boldsymbol{\tau}^{-1}\mathbf{d}\mathbf{z}^* \circ (\mathbf{1} - \mathbf{d}\mathbf{z}^*)) K$$

We have thus obtained a general expression for the Jacobian of the Wilson-Cowan model on graphs, which should hold also for non-homogeneous steady states and/or space-dependent parameters. In order to evaluate the linear stability of any steady state obtained as a solution to the steady state equation (Eqn. 36), it is sufficient to plug it in Eqn. 42 and study the eigenspectrum of the resulting Jacobian.

4.2.3. Explicit Expressions for Jacobian Eigenvalues. — On the human connectome graph, the Jacobian of Eqn. 42 is a dense matrix with more than 10^8 elements, which makes a brute-force numerical approach the only possible route to determine its eigenspectrum. Such a calculation is computationally intensive (although it could be simplified by adopting one of the many algorithms to find only the top-bottom eigenvalues of the spectrum), and would have to be repeated for any parameter set and any steady state under examination. Therefore, it makes sense to attempt to find a more efficient way to calculate the Jacobian eigenspectrum. Indeed, if we restrict the problem to homogeneous steady states and space-independent model parameters, it is possible to obtain an analytic expression for the Jacobian eigenspectrum. Furthermore, these assumptions can be relaxed to allow for *eigenmode-dependent* steady states and model parameters. Define the scalar, steady-state-dependent parameters:

$$(43) \quad a = d_E E^*(1 - d_E E^*), \quad b = d_I I^*(1 - d_I I^*)$$

We can write out the general Jacobian of Eqn. 42, with Gaussian kernels, and under the assumptions

of homogeneous steady state and space-independent model parameters, as follows⁽⁷⁾:

$$(44) \quad J(\mathbf{z}^*) = - \begin{bmatrix} d_E/\tau_E & 0 \\ 0 & d_I/\tau_I \end{bmatrix} \otimes \mathbb{1}_N + \begin{bmatrix} U & 0 \\ 0 & U \end{bmatrix} \begin{bmatrix} a\alpha_{EE}e^{t_{EE}\Lambda}/\tau_E & -a\alpha_{IE}e^{t_{IE}\Lambda}/\tau_E \\ b\alpha_{EI}e^{t_{EI}\Lambda}/\tau_I & -b\alpha_{II}e^{t_{II}\Lambda}/\tau_I \end{bmatrix} \begin{bmatrix} U^T & 0 \\ 0 & U^T \end{bmatrix}$$

From this expression, the decoupling of eigenmodes which will allow us to find explicitly the Jacobian eigenvalues may already be apparent. More to the point, we can use the Jacobian in this form to write the explicit (linearized) equations for the time-evolution of a perturbation about a (homogeneous) steady state:

$$(45) \quad \tau_E \dot{\mathbf{E}}(\mathcal{G}, t) = -d_E \mathbf{E}(\mathcal{G}, t) + a\alpha_{EE}U e^{t_{EE}\Lambda} U^T \mathbf{E}(\mathcal{G}, t) - a\alpha_{IE}U e^{t_{IE}\Lambda} U^T \mathbf{I}(\mathcal{G}, t)$$

$$(46) \quad \tau_I \dot{\mathbf{I}}(\mathcal{G}, t) = -d_I \mathbf{I}(\mathcal{G}, t) + b\alpha_{EI}U e^{t_{EI}\Lambda} U^T \mathbf{E}(\mathcal{G}, t) - b\alpha_{II}U e^{t_{II}\Lambda} U^T \mathbf{I}(\mathcal{G}, t)$$

Now, recall that we have defined the graph-Fourier transform in Eqn. 14 as a multiplication from the left by the graph Laplacian row eigenvectors U^T so for any vector $\mathbf{X}(\mathcal{G}, t)$ on the graph, $U^T \mathbf{X}(\mathcal{G}, t) = \beta^X(\lambda_k, t)$ is the graph Fourier transform. Assuming space-independent model parameters or at best *eigenmode-dependent*⁽⁸⁾ parameters, the linearized Wilson-Cowan equations are diagonalized by the graph Fourier transform (much like the damped-wave equation in Section 3.3.2). Each eigenmode therefore behaves independently like the following 2-dimensional system:

$$(47) \quad \tau_E \dot{\beta}_k^E(t) = (-d_E + a\alpha_{EE}e^{t_{EE}\lambda_k})\beta_k^E(t) - a\alpha_{IE}e^{t_{IE}\lambda_k}\beta_k^I(t)$$

$$(48) \quad \tau_I \dot{\beta}_k^I(t) = b\alpha_{EI}e^{t_{EI}\lambda_k}\beta_k^E(t) - (d_I + b\alpha_{II}e^{t_{II}\lambda_k})\beta_k^I(t)$$

It is now easy to obtain an expression for the Trace and Determinant of the Jacobian of the k^{th} eigenmode:

$$(49) \quad \text{Tr}(J(\mathbf{z}^*))_k = \left(\frac{a}{\tau_E} \alpha_{EE}e^{t_{EE}\lambda_k} - \frac{b}{\tau_I} \alpha_{II}e^{t_{II}\lambda_k} \right) - \left(\frac{d_E}{\tau_E} + \frac{d_I}{\tau_I} \right)$$

$$(50) \quad \text{Det}(J(\mathbf{z}^*))_k = \left(\frac{a}{\tau_E} \alpha_{EE}e^{t_{EE}\lambda_k} - \frac{d_E}{\tau_E} \right) \left(-\frac{b}{\tau_I} \alpha_{II}e^{t_{II}\lambda_k} - \frac{d_I}{\tau_I} \right) + \frac{ab}{\tau_E \tau_I} \alpha_{IE} \alpha_{EI} e^{(t_{EI}+t_{IE})\lambda_k}$$

Finally, the eigenvalues of each eigenmode in terms of their trace and determinant are given by

$$(51) \quad \lambda_{1,2}^{J_k} = \frac{\text{Tr} \pm \sqrt{\text{Tr}^2 - 4\text{Det}}}{2}$$

Note that we have used Gaussian kernels in the derivation, but the result can be straightforwardly generalized to all other kernels. We have thus obtained an analytic prediction for the full eigenspectrum of the Jacobian in the case of homogeneous steady state and space-independent (or eigenmode-dependent) parameters. More specifically, we know the eigenvalue pairs for each eigenmode separately. Thanks to their independence, we can use this information to infer the linear dynamics of a perturbation for each eigenmode.

⁽⁷⁾The assumptions are required because generally space-dependent parameters would be expressed by a non-constant diagonal matrix that would not commute with U .

⁽⁸⁾Eigenmode-dependent parameters would be expressed by a diagonal matrix in the graph Fourier domain, therefore commuting with U .

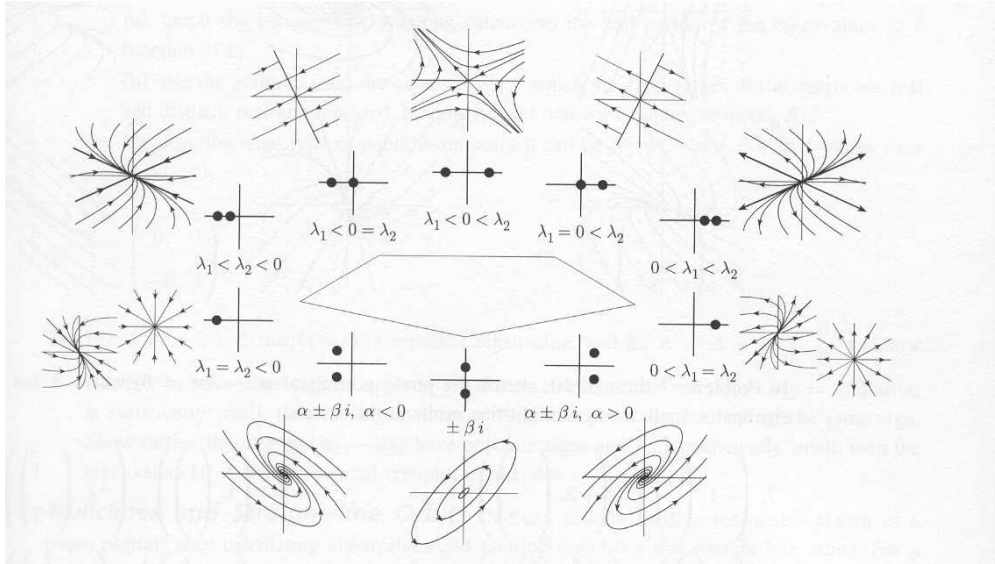


FIGURE 13. A graphical representation of the linear stability of steady states for 2-dimensional systems, in terms of their Jacobian eigenvalues on the complex plane.

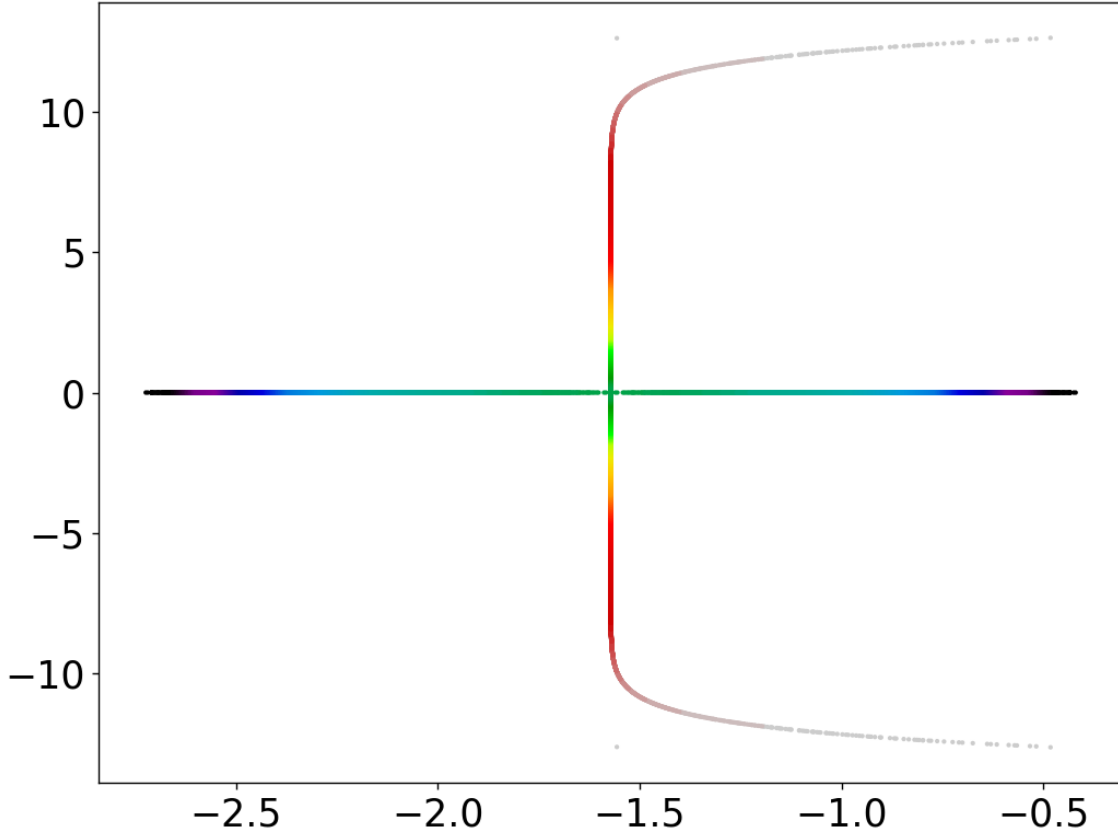


FIGURE 14. The Jacobian eigenspectrum for the Wilson-Cowan model on the connectome graph, with the parameter set of Table 4, on the complex plane, color-coded by eigenmode. For this parameter set, the model has only one steady state, $E^* = 0.0076$ and $I^* = 0.0461$. For this steady state, all Jacobian eigenvalue pairs are either negative reals, or have negative real parts and non-zero imaginary components. The steady state is therefore a stable node for some eigenmodes, and a stable spiral for others. Overall, the steady state should therefore be stable to perturbations. The existence and stability of the steady state are verified by numerical simulations. Furthermore, this result suggests that the system might be in the proximity of a Hopf bifurcation. However, we do not attempt a full bifurcation analysis for time constraints and the high-dimensionality of the parameter space.

5. Equilibrium Fluctuations in the Stochastic Wilson-Cowan Model on Graphs

5.1. Spatiotemporal Power Spectrum. — The concept of (temporal) power spectrum is ubiquitous in signal analysis. In the context of brain data, the expression is most often used for EEG and MEG recordings, to characterize the temporal frequency content of brain oscillations (famously subdivided in alpha, beta, gamma for different ranges of temporal frequencies). In general, the notion of power spectrum is based on Fourier transforming the signal to a more interesting frequency domain, and calculating the variance of fluctuations about a steady state at each frequency. The notion of temporal power spectrum can be straightforwardly extended to a continuous spatial domain; but of more interest to the current work, also to the graph setting, since the graph Fourier transform is defined through the graph Laplacian eigenvectors. The eigenvectors of the connectome-graph Laplacian (the "connectome harmonics") are of practical interest because they may be related to human resting state networks [3]; and of theoretical interest because they can be considered analogues of the Fourier basis on the connectome graph. It may therefore be instructive to study brain activity in these terms [2, 4].

Beyond the connectome-wide spatial power spectrum, it is also possible to analytically obtain a bidimensional *spatiotemporal* power spectrum of noise-induced linear fluctuations about a steady state of the Wilson-Cowan model. This analytic prediction can then be checked by numerical simulations, and suitably transformed and coarse grained in time and space to be compared with multimodal neuroimaging measures of resting-state brain activity. This is a novel approach for a connectome-wide neural field model implemented with the graph Laplacian framework, and may be employed as a stringent test for models claiming to realistically capture the spatiotemporal dynamics of brain activity.

We can go now back to the previously derived linearized Wilson-Cowan model in the graph Fourier domain (Eqns. 47-48), with Gaussian kernels and the scalar, steady state dependent parameters $a = d_E E^*(1 - d_E E^*)$, $b = d_I I^*(1 - d_I I^*)$. Adding a noise term⁽⁹⁾ we obtain the stochastic, linearized equations:

$$(52) \quad \tau_E \dot{\beta}_k^E(t) = (-d_E + a\alpha_{EEE} e^{t_{EE}\lambda_k}) \beta_k^E(t) - a\alpha_{IE} e^{t_{IE}\lambda_k} \beta_k^I(t) + \sigma \xi_k^E(t)$$

$$(53) \quad \tau_I \dot{\beta}_k^I(t) = b\alpha_{EI} e^{t_{EI}\lambda_k} \beta_k^E(t) - (d_I + b\alpha_{II} e^{t_{II}\lambda_k}) \beta_k^I(t) + \sigma \xi_k^I(t)$$

The full spatiotemporal power spectrum can be obtained as follows. Rewriting as the two-dimensional Langevin system for the k^{th} eigenmode:

$$(54) \quad \frac{d}{dt} \beta_k(t) = -A(\lambda_k) \beta_k(t) + \sqrt{D} \xi_k(t),$$

The *temporal* Fourier transform of β_k at angular frequency ω is given by:

$$(55) \quad \beta_k(\omega) = [i\omega I + A(\lambda_k)]^{-1} \sqrt{D} \xi_k(\omega).$$

Abbreviating $M = [i\omega I + A(\lambda_k)]^{-1}$, the cross-spectral matrix $S_k(\omega)$ of β_k is hence given by:

$$(56) \quad S_k(\omega) = \mathbb{E}[\beta_k(\omega) \beta_k(\omega)^\dagger] = M \sqrt{D} \mathbb{E}[\xi_k(\omega) \xi_k(\omega)^\dagger] \sqrt{D} M^\dagger = M D M^\dagger,$$

where, \dagger denotes the conjugate transpose. In the last step we have assumed that ξ_k models uncorrelated temporally-white noise processes with unit variance. We now have a formula for the spatiotemporal power of the excitatory and inhibitory activity, as the elements on the diagonal of $S_k(\omega)$. In terms of the elements of the matrices $A(\lambda_k)$ and D and the angular frequency ω , the spatiotemporal power of excitatory activity for the k^{th} eigenmode is:

⁽⁹⁾Note that the (graph) Fourier transform of a white noise realization is also a white noise realization.

$$(57) \quad [S_k(\omega)]_{00} = \frac{D_{00}(A_{11}^2 + \omega^2) + A_{01}^2 D_{11}}{(A_{00}A_{11} - A_{01}A_{10} - \omega^2)^2 + \omega^2(A_{00} + A_{11})^2}$$

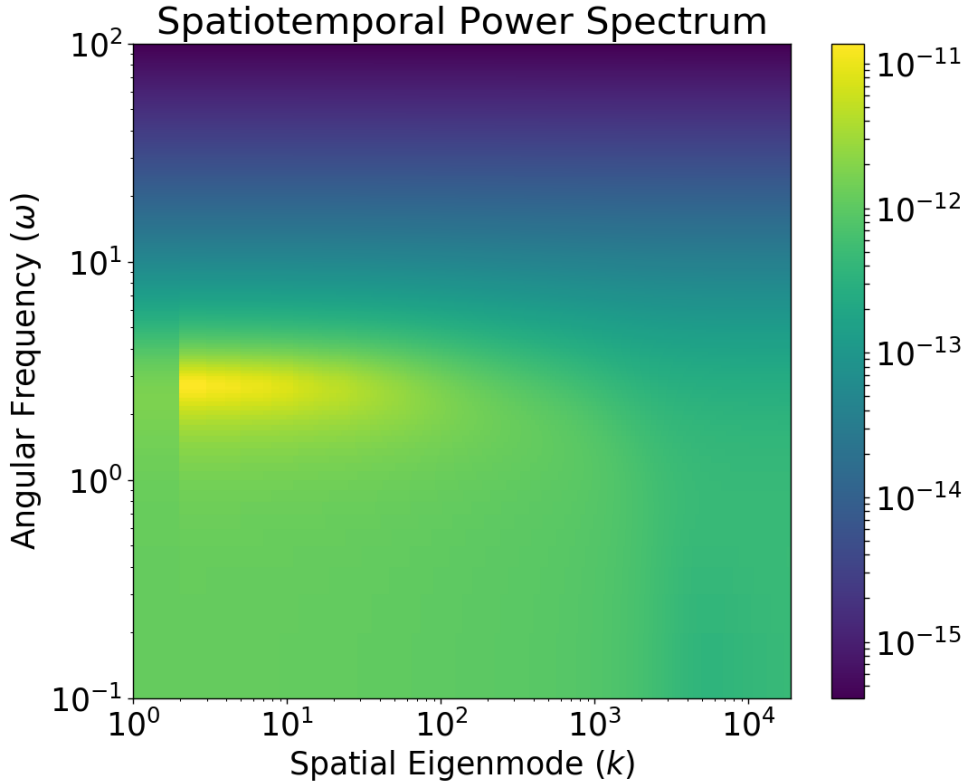


FIGURE 15. The 2D spatiotemporal power spectrum $[S_k(\omega)]_{00}$ of excitatory activity fluctuations about the steady state ($E^* = 0.0076$, $I^* = 0.0461$), for the Wilson-Cowan model on the connectome graph, with the parameter set of Table 4.

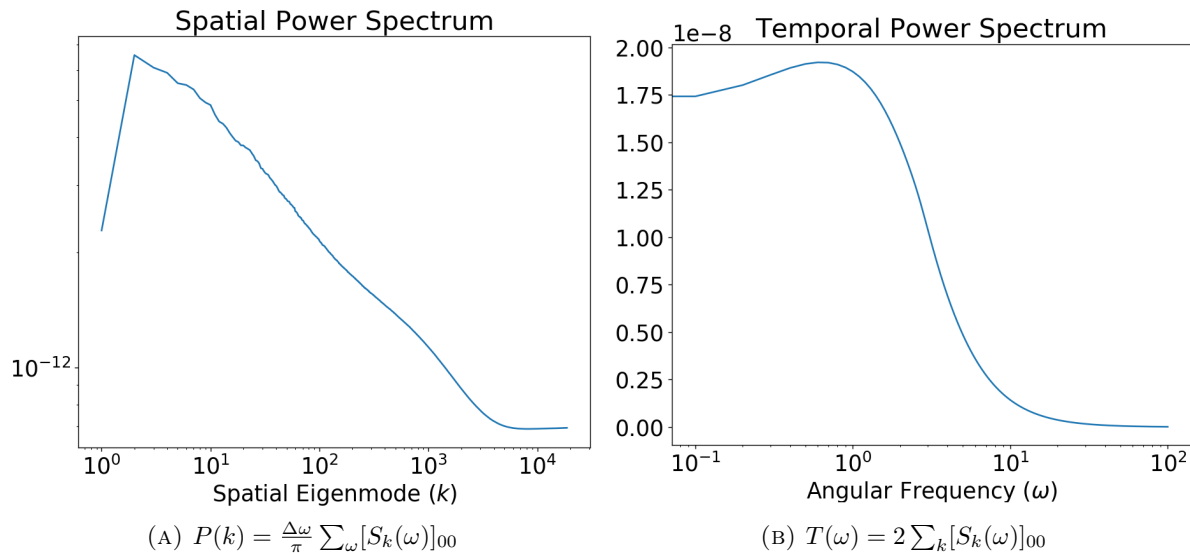


FIGURE 16. Spatial $P(k)$ and temporal $T(\omega)$ power spectra obtained through the 2-dimensional spatiotemporal spectrum formula. Note that the spatial power spectrum is on a log-log scale.

Integrating the 2-dimensional spatiotemporal power spectrum of Figure 15 over the angular frequency ω gives the spatial power spectrum, Figure 16(A); conversely, summing up over all spatial eigenmodes gives the full temporal power spectrum of the system, Figure 16(B). Note that in principle, temporally colored noise could be used as well, and the noise variance can be made eigenmode-dependent if desired. In Appendix A.1, we employ a result from Ornstein-Uhlenbeck statistics to derive an explicit expression for the spatial power spectrum (Eqn. 66); the result is in agreement with that obtained from the 2-dimensional spatiotemporal spectrum.

5.2. Functional Connectivity. — To construct the covariance matrix of excitatory activity across all graph vertices $\Sigma_{\mathcal{G}}$, we first need to construct the covariance matrix Σ_{β} in the graph Fourier domain. Because of the independence of eigenmodes, the covariance matrix (at lag zero) in the graph Fourier domain Σ_{β} is simply a diagonal matrix of size N with the elements along the diagonal being the values of the spatial power spectrum.

$$(58) \quad \Sigma_{\beta} = \text{Diag}(P(k))$$

The covariance matrix across all vertices is obtained by transforming back to the vertex domain:

$$(59) \quad \Sigma_{\mathcal{G}} = U \Sigma_{\beta} U^T$$

The correlation matrix C , which is often used in fMRI resting-state functional connectivity studies, is obtained simply by normalizing the covariance matrix

$$(60) \quad C = (\Sigma_{\mathcal{G}}^+)^{-1/2} \Sigma_{\mathcal{G}} (\Sigma_{\mathcal{G}}^+)^{-1/2},$$

where $\Sigma_{\mathcal{G}}^+$ denotes $\Sigma_{\mathcal{G}}$ with all off-diagonal entries set to zero. Seed-based connectivity of the j -th node is measured by the j -th row (or column) of C . In principle, it would be possible to spatiotemporally coarse-grain the predicted functional connectivity matrix of the model for comparison with empirical fMRI data, but we do not attempt this here for temporal constraints. Fitting the functional connectivity matrix would represent a stringent constraint on the model dynamics, and might be employed in future work to identify biologically suitable models and parameter sets.

5.3. Comparison with Empirical Data. — The spatiotemporal power spectra and functional connectivity of model dynamics thus obtained may be thought of being relevant at the level of electrochemical neural activity; in turn, this must be suitably transformed to reflect what is actually measured with neuroimaging methods (scalp recordings for EEG, BOLD signal for fMRI). For simplicity, here we focus only on a qualitative comparison with existing data for spatial fMRI measures. We use this procedure in order to identify the parameter set reported in Table 4. The comparison with fMRI functional connectivity and EEG/MEG spectra is an equally interesting potential direction for future work.

5.3.1. Wilson-Cowan Model vs fMRI Spatial Power Spectra. — In [4], an empirical spatial power spectrum of resting-state BOLD fMRI fluctuations is calculated, in terms of connectome-graph Laplacian eigenvectors, and changes induced by LSD administration are studied. It is important to note that 1) the definition of power used in [4] is not in agreement with the standard definition used here (variance of fluctuations about a steady state in the graph Fourier domain), and 2) the graph-Laplacian employed in that paper is not metric, but rather weighted according to group-averaged white matter tracts. Our preferred choice of a metric graph Laplacian preserves the connection with neural field equations, as previously mentioned in Section 3.

The BOLD fMRI response is well known to correlate with neural activity [40], despite some important caveats [1, 12]. The relation between neural activity and BOLD response is often modeled with a temporal convolution with a hemodynamic response function. Hemodynamic delay and temporal smoothing should have no effect on the power spectrum, since in principle we are always

analyzing fluctuations about a steady state. Similarly, the spatial smoothing is implied by the fact that we restrict the comparison between model and empirical data to those eigenmodes that could be reliably observed with fMRI ($k = 2 - 5000$). Therefore, in very simplistic terms, we model the fMRI spatial power spectrum as a rescaled version of the excitatory activity power spectrum predicted by the Wilson-Cowan model on the connectome graph.

5.3.2. Parameter Set Identification. — We employ a variant of the basin hopping fitting algorithm [46] implemented in Python (see online code for full details, link in Appendix A.3). This allows us to find a parameter combination that gives a spatial power spectrum reasonably similar to the empirically observed one, while avoiding local minima of the optimization function. The optimization function is simply the 2-norm of the distance between the model power spectrum, in log-log coordinates, and the best-fit line to the empirical power spectrum in the range $k = 2 - 5000$. The optimal scaling parameter $\alpha = 171.1$ is identified automatically by the fitting procedure. The best parameter set obtained by multiple iterations⁽¹⁰⁾ of this procedure is that reported in Table 4. Due to the high dimensionality of the parameter space, a systematic exploration is not carried out, and therefore we note that there might be other equally or more suitable parameter sets. Furthermore, the optimization was only performed for the Wilson-Cowan model with four Gaussian kernels. It is probable that different kernel choices or combinations thereof would yield even better results.

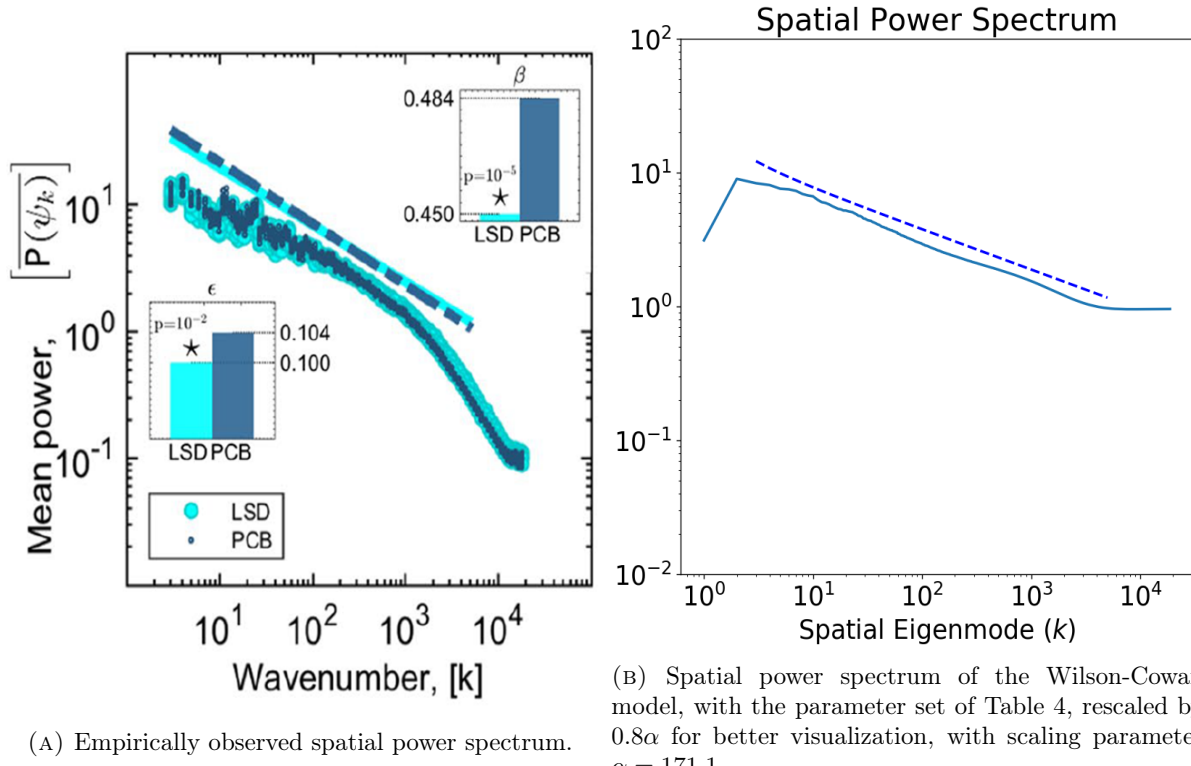


FIGURE 17. Comparison between Wilson-Cowan power spectrum and empirical data from [4]. Note that we only fit the spectrum for eigenmodes within the range of the best-fit line ($k = 2 - 5000$).

(B) Spatial power spectrum of the Wilson-Cowan model, with the parameter set of Table 4, rescaled by 0.8α for better visualization, with scaling parameter $\alpha = 171.1$.

⁽¹⁰⁾With the parameter set used in [3], or the results of previous optimizations, as starting point.

6. Numerical Simulations of the Stochastic Wilson-Cowan Model on Graphs

The main numerical results of this work comprise of two parts: nonlinear simulations of the stochastic Wilson-Cowan model (Eqns. 33-34) on a regular 1-dimensional graph; and simulations of the linearized stochastic Wilson-Cowan model (Eqns. 47-48) on the full human connectome graph. Numerical tests are a crucial step to validate any analytic prediction, from the existence and stability of a steady state, to the spatiotemporal spectra. In fact, it is indeed possible to obtain (virtually meaningless) analytic predictions for the power spectra of noise-induced fluctuations about *unstable* steady states. As mentioned in Section 5.3, we select the parameter set for numerical simulations to qualitatively match the spatial power spectrum of fMRI data reported in [4]. The spatial power spectrum of numerical simulations is measured as the variance of fluctuations of excitatory activity about the steady state, in the graph Fourier domain; the temporal power spectrum is simply measured with the Python built-in periodogram function.

We report results only for the model with four Gaussian kernels, because the parameter search algorithm of Section 5.3 was restricted to this case, but it is straightforward to obtain analytic predictions and carry out identical numerical tests for non-Gaussian kernels. Note that the choice of kernel does not influence the steady state values, because kernels do not appear in the (homogeneous) steady state equation (Eqn. 37); however, kernels do appear in the Jacobian eigenspectrum and in the spatiotemporal spectra. Therefore, kernel choice directly affects the spatiotemporal power spectrum, and potentially may even altogether change the stability character of a steady state.

6.1. Nonlinear Simulations on a Regular One-Dimensional Graph. — Measured spatial and temporal power spectra of nonlinear simulations of the stochastic Wilson-Cowan model with Gaussian kernels and the parameter set of Table 3, on a regular one-dimensional graph of unitary spacing, are reported in Figure 18. The numerical results appear in excellent agreement with the analytic prediction, thereby also confirming the existence and stability of the steady state for this parameter set and kernel choice.

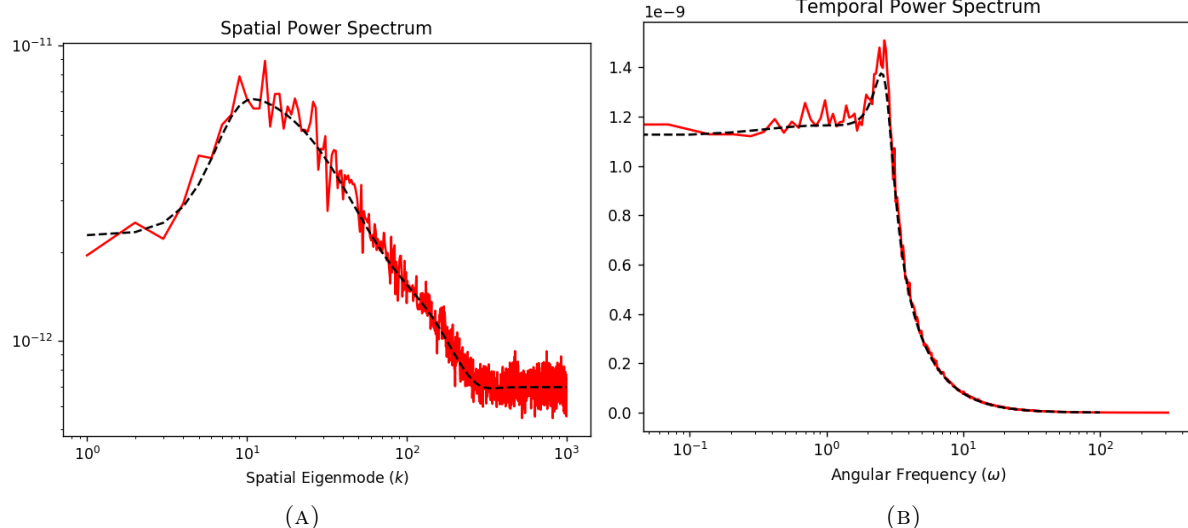


FIGURE 18. Comparison of analytic prediction (black, dashed) and numerical simulation (red) for the spatial (A) and temporal (B) spectra of the Wilson-Cowan model on a regular, one dimensional graph, with the parameter set of Table 4.

6.2. Linearized Simulations on the Human Connectome Graph. — In order to make numerical simulations of the Wilson-Cowan model on the full human connectome graph feasible on a regular commercial machine, we take advantage of the fact that in the linearized Wilson-Cowan model each graph Laplacian eigenmode behaves like an independent 2-dimensional Langevin system. Therefore

we are able to efficiently⁽¹¹⁾ simulate the (linearized) dynamics of each eigenmode, without approximating the activity propagators. With this implementation, it is possible to expediently simulate the linearized, stochastic Wilson-Cowan model on the full human connectome graph, and obtain the connectome-wide spatial and temporal spectra. If needed, it is also possible reconstruct the activity pattern on the full human connectome graph simply by applying the inverse graph Fourier transform, for example to calculate the functional connectivity. The connectome-wide power spectra measured in numerical simulations appear in excellent agreement with the analytic predictions. The results for the model with Gaussian kernels and the usual parameter set of Table 4 are reported in Figure 19.

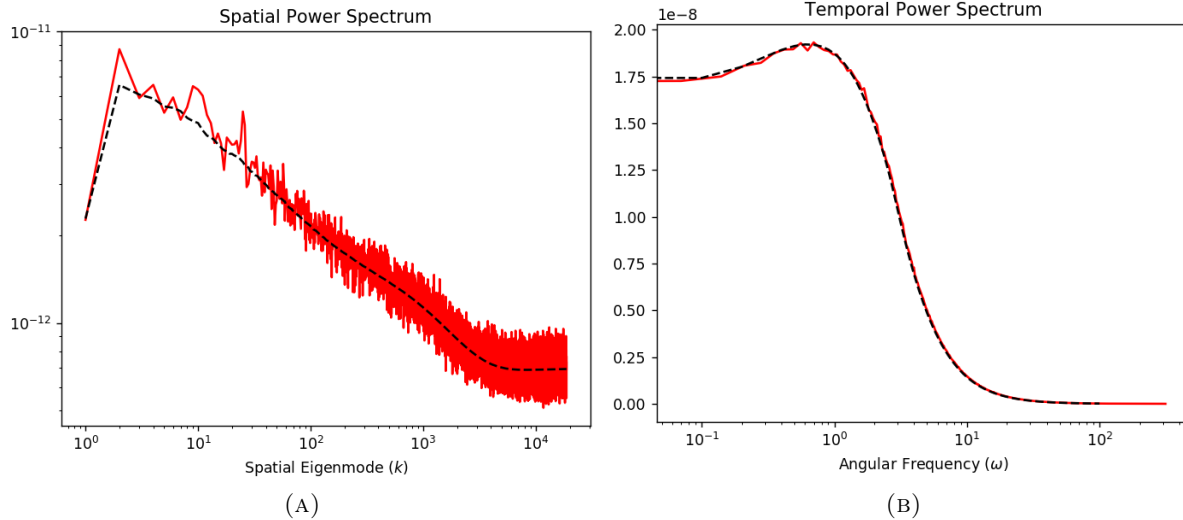


FIGURE 19. Comparison of analytic prediction (black, dashed) and numerical simulation (red) for the spatial (A) and temporal (B) spectra of the linearized Wilson-Cowan model on the human connectome graph, with Gaussian kernels and the parameter set of Table 4.

⁽¹¹⁾On a laptop with 16GB of RAM, full-connectome numerical simulations of 10000 timesteps, with $\delta t = 0.01$, were completed in few minutes.

7. Discussion

7.1. The Wilson-Cowan Model of Atasoy et al. — It is important to discuss the current work in relation to [3], the first graph Laplacian-based approach to neural field models on the human connectome, because our implementation can be considered a direct theory-driven extension and generalization of the modeling work carried out therein. We address several limitations of the Wilson-Cowan model proposed in [3]: first, the unweighted graph Laplacian is substituted here by a *metric* graph Laplacian, through which physical distances of activity propagation between nodes are directly incorporated in the model. The unweighted graph Laplacian is a topological invariant of the graph, and physically meaningless in this context, because it does not maintain the analogy with continuous neural fields. Another improvement is the generalization of the activity propagators to non-Gaussian convolution kernels, and time-evolution operators (e.g. the damped wave) of ordinary differential equations on graphs. This is a novel result (to our knowledge) in the context of neural activity models on graphs. Finally, we include in the model formulation terms for subcortical input, and crucially, *noise*. The addition of a noise term makes our equations *stochastic*, rather than deterministic as in [3], and allows further analytic progress in the study of the model dynamics on the human connectome, particularly the characterization of resting state activity as noise-induced fluctuations about a steady state. Limit-cycles, the focus of [3], are commonly associated with pathological epileptic dynamics, whereas noise-induced fluctuations are more akin to healthy resting-state brain dynamics.

Mathematical Analysis. — We present a general and a space-independent linear stability analysis, correcting also a small imprecision found in the calculation of the system steady states in the Supplementary Materials of [3] (see Section 4.2.1 for details), which might compromise the reliability of their analytic results. Moving beyond linear stability analysis, we obtain spatiotemporal power spectra and functional connectivity structures of noise-induced equilibrium fluctuations for the Wilson-Cowan model on the human connectome graph. These predictions are verified quantitatively via numerical simulations and qualitatively by comparison with neuroimaging data (the latter only for spatial spectra). We note also that the definition of power used in [4] does not appear in agreement with the standard definition used here.

Numerical Simulations. — Simulating a nonlinear, stochastic neural field model on a high-resolution human connectome graph is computationally expensive, but nonetheless already feasible on present-day clusters or supercomputers. To address this constraint, Atasoy et al. effectively implemented numerical simulations with a first-order approximation of the propagator matrices, in that case graph Laplacian matrix exponentials, equivalent to the forward-time finite-difference approximation of the diffusion equation. Here, we start by implementing nonlinear simulations on a one-dimensional regular graph with 1000 nodes, in order to test the correctness of the approach and the validity of analytic predictions. Next, in order to make full-connectome numerical simulations feasible on a regular commercial machine, we take advantage of the decoupling of the linearized Wilson-Cowan model in the graph Fourier domain, which implies that each graph Laplacian eigenmode behaves like an independent 2-dimensional system. This approach has the advantage of not requiring any approximation of the propagators, but is restricted to the case of space-independent or at best eigenmode-dependent parameters, as discussed in Section 4.2.3.

7.2. Neural Mass Models. — The main advantage of the graph Laplacian framework with respect to current neural mass-network models is perhaps the possibility of explicitly modeling activity propagation on the human connectome graph, moving beyond the more abstract "coupling" concept. Biophysically realistic models of neural population dynamics and activity propagation may be implemented on connectomes with high spatial resolution, while maintaining tractability for mathematical analysis (and numerical simulations). In particular, previous studies [15] have emphasized the key role of coupling and delay among regions in order to obtain realistic dynamics with neural mass models. The graph-Laplacian framework allows for explicit modeling of activity propagation (including delays) in a natural way. It is not in principle necessary to artificially specify local dynamics (e.g. tuned to be 40hz oscillations as in some cases) or the strength of coupling between nodes/regions. Instead, the graph structure is simply based on structural connections and their length, either along white matter fibers, or Euclidean for local connections. Furthermore, maintaining the possibility for sufficiently

accurate mathematical analysis (as shown by the excellent agreement between analytic prediction and numerical measurements of spatiotemporal spectra reported in Section 6) means that the approach is easily scalable to connectomes of much higher spatial resolution than the one used in the present study. Whereas instead, approaches based solely on numerical simulations (such as the Virtual Brain) become less and less feasible as the spatial resolution of the underlying structural connectome graph increases.

7.3. Neural Field Models. — In comparison with existing neural field models, the first significant improvement of this framework can be found in its relatively simple and minimal mathematical formulation. The state-of-the-art work on neural field models has reached a high level of mathematical specialization, allowing great progress and discovery. But in turn, this has made the understanding and checking of each step and premise prohibitive for experimental neuroscientists, or even mathematical neuroscientists working within different frameworks (let alone comparison between different approaches). In perspective, implementing a neural field model directly on a high-resolution connectome may be more natural and closer to the biological system than approximating the human cortical network as a flat sheet or a sphere (which nonetheless proved to be a very useful and powerful approximation). This also avoids the additional complexity of accounting post-hoc for cortical folding, and potentially makes it feasible to account for cortical thickness and cortical layers, which can already be distinguished in present-day structural and functional MRI data. Grey matter (local), white matter (nonlocal) interhemispheric, and intrahemispheric connections can all be included naturally in the metric graph Laplacian, with no requirements for symmetry or homogeneity of connectivity. Unlike most current neural field models, it becomes also possible to account for individual structural differences by using subject-specific connectomes, and study their consequences for functional organization.

7.4. Limitations. — Nonetheless, there are certainly limitations to this approach, and clearly even more so to this specific thesis. The main general limitation of the approach is perhaps the difficulty of analysis for models with arbitrarily space-dependent parameters. The space-independent parameters approximation has also been used in previous modeling studies, and has the advantage of making the analytic results presented here virtually "infinitely" scalable to more detailed connectomes. However, there are more biophysically realistic models that would require space-dependent parameters. For example, some models incorporate neuronal receptors and their densities, which are known to vary across the cortex. This limitation might be overcome with a hybrid approach of space-dependent numerical simulations and space-independent analysis, or by attempting to absorb all the relevant space-dependent information into the graph Laplacian matrix, but the outcome is not clear at present. Another limitation is the use of an undirected (weighted) and time-independent connectome graph. For maximal generality, one might want to study a directed, or even time-dependent (plastic) structural connectome: it is not clear if this can be implemented in the current framework.

For what concerns the limitations of this specific thesis, it is important to note that we study a unit-less version of the Wilson-Cowan model, which has the drawback that the model parameters cannot be directly related to any biophysical property of the system. In terms of parameter-space exploration and comparisons with empirical data, we note that we chose the parameter set for analysis and simulation by fitting the analytically predicted spatial power spectrum to the (log-log) best-fit line of the empirical spatial power spectrum of resting-state brain activity, restricted to the Wilson-Cowan model with Gaussian kernels⁽¹²⁾. We do not perform a quantitative fitting to the actual empirical data; we do not compare the model temporal spectrum with empirical data, nor its functional connectivity, nor we take into account neuroimaging modalities other than fMRI.

⁽¹²⁾A minor practical limitation of the current formulation is that the kernel parameter does not have the same meaning for all kernels. This should be addressed in future work to allow more expedient comparison of the effect of different kernels on the model dynamics.

8. Conclusion and Future Work

In summary, in this thesis we have presented a mathematical and computational theory-driven framework based on the graph Laplacian formalism, for the study of neural activity models on the human connectome graph, as a hybrid approach between neural fields and masses. As an example, we have studied a stochastic Wilson-Cowan model, showing excellent agreement between analytic predictions and numerical simulations, and that even this simple model is capable of reproducing the spatial power spectrum of fMRI data.

There are several attributes of this framework making it attractive for the development and implementation of next-generation models of neural activity. First, it is amenable to scalable mathematical and computational analyses. Second, the framework is relatively "minimal" in its mathematical formulation, relying mainly on the quality and spatial resolution of the structural connectome, which is ever-increasing thanks to advances in MRI field strengths and analysis techniques; and on the chosen model for cortical activity generation and propagation, of which many examples are available and have been studied on regional networks or continuous domains. Third, the flexibility of this framework allows for countless "cross testing" combinations of modeling and analysis methods. The properties of models implemented in this framework may be assessed with a variety of different methods: from mathematical techniques developed for the study of continuous neural field models, which may be translated to the graph domain (e.g. characterization of waves and bumps), to methods from the field of discrete signal processing on graphs, and other emergent characterizations of brain activity (e.g. lagged functional connectivity, cortical waves, studies of functional and structural networks from the perspective of graph theory and algebraic topology).

Novel analysis methods may therefore be tested in a "controlled" environment (surrogate data may be obtained by randomizing long-range connections as in [3] or by other means); in turn, novel models implemented in this framework may be compared to data from multiple neuroimaging modalities, and examined with a variety of previously validated methods. Models claiming to be realistic, or different parameter sets within one model, may be put to direct test to determine their range of application, and the validity (as well as fundamentality) of their underlying theoretical principles and assumptions; in turn, this may lead to evolution and development of new models. In regard to biophysical realism, we do not make such claims for the current model, which is rather presented as an interesting example of the possibilities allowed by graph Laplacian framework. The formulation of a satisfactory account of neural activity would require a model with biophysical (not unit-less) parameters, and quantitative comparisons with multiple neuroimaging modalities (fMRI, MEG,...), ideally for qualitatively different neural states (e.g. wakefulness, anesthesia, psychedelic-state). Once an optimized model is obtained, it would also be interesting to study the response of the model to an incoming "stimulus", as has been done previously for continuous neural field models.

More specifically, it is certainly worth remarking that thanks to the implementation on the connectome, the framework may be used to develop and study anatomically individualized (and condition-specific) models, thereby allowing the study of the effects of individual differences in structural anatomy and connectivity on functional organization, both in health and pathology, an important question in modern psychiatry [19]. Crucially, the connectome harmonics (eigenvectors of the connectome graph Laplacian) provide a unified language [2] which can be used to translate and compare results across individuals and conditions. It is important to also note that the framework need not be applied to whole-brain models, but may also find application to modeling the dynamics of specific regions. For example, the primary visual cortex may be of particular interest in this sense, because of the known mapping between patterns of neural activity in this region and visual (retinotopic) percepts. Another potentially interesting direction of future work may be the application of this framework to MEG source modeling i.e. identification of the source of MEG signals recorded on the scalp. To this end, one would first translate the neural activity on the connectome into MEG scalp signals, and fit model parameters to existing MEG data, and finally attempt to use the resulting model to reconstruct the neural source of MEG signals. This procedure may be used as stand-alone, or to offer model-based validation to the results of other analysis methods.

In conclusion, we hope that this work may provide some interesting considerations and an initial exploration of the graph Laplacian framework for neural field models. Because of the vast possibilities allowed by this framework, it is only through rigorous examination from multiple perspectives that its potential may be developed. We hope that other authors, from mathematical to experimental and clinical neuroscientists, will join in the discussion to help us understand how much light (if any) this approach may shed on the structure-function relation in the human brain.

Appendix

A.1 Spatial Power Spectrum with Ornstein-Uhlenbeck Method. — An explicit expression for the spatial power spectrum of the Wilson-Cowan model can be found as follows. Indicating with the subscript k that we are treating the k^{th} eigenmode (the connectome harmonic with eigenvalue λ_k), we rewrite the system in the form

$$(61) \quad \frac{d}{dt} \begin{bmatrix} \beta_k^E(t) \\ \beta_k^I(t) \end{bmatrix} = -A(\lambda_k) \begin{bmatrix} \beta_k^E(t) \\ \beta_k^I(t) \end{bmatrix} + \sqrt{D} \begin{bmatrix} \xi_k^E(t) \\ \xi_k^I(t) \end{bmatrix}$$

Explicitly, in our case we have

$$(62) \quad A(\lambda_k) = \begin{bmatrix} \frac{d_E}{\tau_E} - \frac{a}{\tau_E} \alpha_{EE} e^{t_{EE}\lambda_k} & \frac{a}{\tau_E} \alpha_{IE} e^{t_{IE}\lambda_k} \\ -\frac{b}{\tau_I} \alpha_{EI} e^{t_{EI}\lambda_k} & \frac{b}{\tau_I} \alpha_{II} e^{t_{II}\lambda_k} + \frac{d_I}{\tau_I} \end{bmatrix} \quad \sqrt{D} = \begin{bmatrix} \sigma/\tau_E & 0 \\ 0 & \sigma/\tau_I \end{bmatrix}$$

This is a Langevin-type system of stochastic differential equations. We can now apply in the graph domain Ornstein-Uhlenbeck method which allow us to obtain the "spatial" (in the sense of the connectome harmonics) power spectrum of noise-induced activity fluctuations about the steady state. This method was originally developed for continuous systems of stochastic differential equations, and previously applied, among others, to chemical reactions [11], a continuous model of cortical dynamics [44], and a microscopic (non-mean-field) 1D version of the Wilson-Cowan model [31].

Define the 2×2 matrix $G(\lambda_k)$, for each eigenmode, as:

$$(63) \quad G(\lambda_k) = \frac{\text{Det}(A)D + (A - \text{Tr}(A) \cdot \mathbf{1}_2)D(A - \text{Tr}(A) \cdot \mathbf{1}_2)^T}{2\text{Tr}(A)\text{Det}(A)}$$

it can be shown [11] that, for a system of equations such as this⁽¹³⁾:

$$(64) \quad \mathbf{G}(\lambda_k, \lambda_{k'}) = \lim_{t \rightarrow \infty} \begin{bmatrix} \langle \beta_k^E(t) \beta_{k'}^E(t) \rangle & \langle \beta_k^E(t) \beta_{k'}^I(t) \rangle \\ \langle \beta_k^I(t) \beta_{k'}^E(t) \rangle & \langle \beta_k^I(t) \beta_{k'}^I(t) \rangle \end{bmatrix} = \delta(\lambda_k - \lambda_{k'}) G(\lambda_k)$$

The spatial power spectral density of excitatory activity for eigenmode k is given by $[G(\lambda_k)]_{00}$. In terms of the elements of the matrices A and D :

$$(65) \quad [G(\lambda_k)]_{00} = \frac{D_{00}(A_{00}A_{11} - A_{01}A_{10}) + A_{11}^2 D_{00} + A_{01}^2 D_{11}}{2(A_{00}A_{11} - A_{01}A_{10})(A_{00} + A_{11})}$$

After some simplifications, we can obtain the following explicit expression for the full spatial power spectrum of excitatory activity, in terms of the model parameters, and generalized to all kernels, expressed in the graph Fourier domain (we write $\beta_{**}(\lambda_k) = \beta_{**}$ for compactness).

$$(66) \quad [G]_{00} = \frac{\sigma^2}{\frac{d_E \tau_I + d_I \tau_E - a \tau_I \alpha_{EE} \beta_{EE} + b \tau_E \alpha_{II} \beta_{II}}{d_E d_I + b d_E \alpha_{II} \beta_{II} - a d_I \alpha_{EE} \beta_{EE} + a b (\alpha_{EI} \alpha_{IE} \beta_{EI} \beta_{IE} - \alpha_{II} \alpha_{EE} \beta_{II} \beta_{EE})}}$$

$$\cdot \frac{1}{2} \left(\frac{\tau_I}{\tau_E} + \frac{a^2 \alpha_{IE}^2 \beta_{IE}^2 + (d_I + b \alpha_{II} \beta_{II})^2}{d_E d_I + b d_E \alpha_{II} \beta_{II} - a d_I \alpha_{EE} \beta_{EE} + a b (\alpha_{EI} \alpha_{IE} \beta_{EI} \beta_{IE} - \alpha_{II} \alpha_{EE} \beta_{II} \beta_{EE})} \right)$$

We note that the square of the noise intensity parameter σ^2 appears in the theoretical expression of the power spectrum as potential scaling parameter; however, in many cases, the Wilson-Cowan model has multiple valid steady states, and if the noise intensity is comparable to the distance between steady

⁽¹³⁾In two of the three previous references where this method is applied, the formula of Eqn. 64 appears with a plus sign: $\delta(\lambda_k + \lambda_{k'})$, without further explanation of the meaning of the symbol δ , and in one reference ([44]), the δ is absent. To the best of our understanding, and in agreement with the latter reference, the term term should be a shifted Dirac delta function representing the uncorrelated noise, and should therefore be noted with a minus sign.

states (i.e. fluctuations are not "sub-threshold"), the system dynamics may straddle across different steady states (multistability). In numerical simulations, this leads to the observation of a "hybrid" power spectrum, qualitatively appearing as a mixture of the power spectra of the different steady states (whereas the analytic prediction is simply rescaled by larger noise intensity). Therefore the noise intensity may not be used as scaling parameter of the spectrum, but this observation may be of relevance since some recent modeling efforts have focused on multistable systems [22]

A.2 Spatiotemporal Power Spectrum of the Continuous Diffusion Equation. — As an instructive example, we derive a formula for the spatial power spectrum of the continuous diffusion equation:

Consider the diffusion equation on the line:

$$(67) \quad \frac{\partial f}{\partial t}(x, t) = D \frac{\partial^2 f}{\partial x^2}(x, t) + \sigma \xi(x, t),$$

where $D > 0$ is the diffusion coefficient, $\xi(x, t)$ denotes spatiotemporal white-noise with unit-variance, and $\sigma > 0$ denotes the intensity of the incoming noise. In the spatiotemporal Fourier domain, the diffusion equation reads

$$(68) \quad i\omega f(k, \omega) = -Dk^2 f(k, \omega) + \sigma \xi(k, \omega).$$

Solving for f gives

$$(69) \quad f(k, \omega) = \frac{\sigma}{i\omega + Dk^2} \xi(k, \omega).$$

Note that $f(k, \omega) = h(k, \omega)\xi(k, \omega)$ can be viewed as linear filter with input $\xi(k, \omega)$, output $f(k, \omega)$, and transfer function

$$(70) \quad h(k, \omega) = \frac{\sigma}{i\omega + Dk^2}.$$

The assumption that ξ is spatiotemporally white means that $\xi(k, \omega) = e^{i\phi(k, \omega)}$, where $\phi(k, \omega)$ is uniformly distributed on $[0, 2\pi]$, independently for every k and ω . The spatiotemporal power spectrum $p(k, \omega)$ of f is given by

$$(71) \quad p(k, \omega) = \|f(k, \omega)\|^2 = \|h(k, \omega)\|^2 = \frac{\sigma^2}{\omega^2 + (Dk^2)^2}.$$

To obtain the wavenumber spectrum, that is, the power spectrum only as a function of k , we integrate $p(k, \omega)$ over ω and obtain

$$(72) \quad p(k) = 2 \int_0^\infty p(k, \omega) d\omega = 2\sigma^2 \int_0^\infty \frac{d\omega}{\omega^2 + (Dk^2)^2} = \frac{2\sigma^2}{Dk^2} \left[\arctan \frac{\omega}{(Dk^2)} \right]_0^\infty = \left(\frac{\pi\sigma^2}{D} \right) \frac{1}{k^2}.$$

We now show that by using a similar calculation, the wavenumber spectrum of the diffusion equation on a graph can be obtained. In the spatiotemporal Fourier domain, the diffusion equation on a graph with Laplacian $L = U^T \Lambda U$:

$$(73) \quad \frac{df}{dt}(t) = DLf(t) + \sigma \xi(t),$$

is given by

$$(74) \quad i\omega \beta^f = D\Lambda \beta^f(\omega) + \sigma \beta^\xi(\omega),$$

where the vectors $\beta^f(\omega)$ and $\beta^\xi(\omega)$ denote the spatiotemporal Fourier transforms of f and ξ , respectively. Solving for $\beta^f(\omega)$ gives

$$(75) \quad \beta^f(\omega) = \sigma [i\omega \mathbf{1} - D\Lambda]^{-1} \beta^\xi(\omega) = h^L(\omega) \beta^\xi(\omega),$$

where $\mathbf{1}$ denotes the identity matrix and $h^L(\omega)$ denotes the transfer function, which is a diagonal matrix with k -th diagonal entry equal to

$$(76) \quad h_{k,k}^L(\omega) = \frac{\sigma}{i\omega - D\lambda_k}.$$

Note that k now indexes the graph-theoretic Fourier basis functions (and not a wavenumber). I use the same letter k just to stress the link with the continuous case. Note that Eq. (20) is the graph-theoretic equivalent of Eq. (14). The k -th coordinate of the spatiotemporal power spectrum $p(\omega)$ of f is thus given by

$$(77) \quad p_k(\omega) = \|\beta_k^f\|^2 = \|h_{k,k}^L(\omega)\|^2 = \frac{\sigma^2}{\omega^2 + D^2\lambda_k^2}.$$

Note that Eq. (22) is the graph-theoretic equivalent of Eq. (16). Integrating over ω yields the wavenumber spectrum p_f of f . Its k -th coordinate equals

$$(78) \quad p_k^f = \left(\frac{\pi\sigma^2}{D} \right) \frac{1}{\lambda_k}.$$

Note that the wavenumber spectrum of diffusion on a graph is related to the wavenumber spectrum of the diffusion equation on the line by replacing $-k^2$ by λ_k . Also note that the wavenumber spectra follow a power-law, although the dynamics are not critical (we are dealing with linear equilibrium fluctuations). The diffusion equation, however, can only generate spectra with a single slope (-2 on the line and -1 on a graph). The Wilson-Cowan equations can instead generate power-law spectra with different shapes and slopes.

A.3 Code. — The Python 3.6 code for all analysis and simulations was developed by Marco Aqil. It is available for use and review under standard MIT license at the link:

<https://github.com/marcoaqil/Graph-Stochastic-Wilson-Cowan-Model/>.

Acknowledgements

M.A. would like to thank Dr. S. Atasoy, Prof. R.Hindriks, Prof. J. Hulshof and Prof. T.Knapen for valuable input and useful discussion during the development of this thesis.

References

- [1] O. J. ARTHURS & S. BONIFACE – “How well do we understand the neural origins of the fmri bold signal?”, *Trends in neurosciences* **25** (2002), no. 1, p. 27–31.
- [2] S. ATASOY, G. DECO, M. L. KRINGELBACH & J. PEARSON – “Harmonic brain modes: a unifying framework for linking space and time in brain dynamics”, *The Neuroscientist* **24** (2018), no. 3, p. 277–293.
- [3] S. ATASOY, I. DONNELLY & J. PEARSON – “Human brain networks function in connectome-specific harmonic waves”, *Nature communications* **7** (2016), p. 10340.
- [4] S. ATASOY, L. ROSEMAN, M. KAELEN, M. L. KRINGELBACH, G. DECO & R. L. CARHART-HARRIS – “Connectome-harmonic decomposition of human brain activity reveals dynamical repertoire re-organization under lsd”, *Scientific reports* **7** (2017), no. 1, p. 17661.
- [5] K. BANSAL, J. NAKUCI & S. F. MULDOON – “Personalized brain network models for assessing structure–function relationships”, *Current opinion in neurobiology* **52** (2018), p. 42–47.
- [6] E. BERTUZZO, R. CASAGRANDI, M. GATTO, I. RODRIGUEZ-ITURBE & A. RINALDO – “On spatially explicit models of cholera epidemics”, *Journal of the Royal Society Interface* **7** (2010), no. 43, p. 321–333.
- [7] R. L. BEURLE – “Properties of a mass of cells capable of regenerating pulses”, *Phil. Trans. R. Soc. Lond. B* **240** (1956), no. 669, p. 55–94.
- [8] M. BREAKSPEAR – “Dynamic models of large-scale brain activity”, *Nature neuroscience* **20** (2017), no. 3, p. 340.
- [9] P. C. BRESSLOFF, J. D. COWAN, M. GOLUBITSKY, P. J. THOMAS & M. C. WIENER – “What geometric visual hallucinations tell us about the visual cortex”, *Neural computation* **14** (2002), no. 3, p. 473–491.
- [10] T. C. BUTLER, M. BENAYOUN, E. WALLACE, W. VAN DRONGELEN, N. GOLDENFELD & J. COWAN – “Evolutionary constraints on visual cortex architecture from the dynamics of hallucinations”, *Proceedings of the National Academy of Sciences* **109** (2012), no. 2, p. 606–609.
- [11] S. CHATURVEDI, C. GARDINER, I. MATHESON & D. WALLS – “Stochastic analysis of a chemical reaction with spatial and temporal structures”, *Journal of Statistical Physics* **17** (1977), no. 6, p. 469–489.
- [12] D. M. COLE, S. M. SMITH & C. F. BECKMANN – “Advances and pitfalls in the analysis and interpretation of resting-state fmri data”, *Frontiers in systems neuroscience* **4** (2010), p. 8.
- [13] S. COOMBES, P. BEIM GRABEN, R. POTTHAST & J. WRIGHT – *Neural fields: theory and applications*, Springer, 2014.
- [14] J. D. COWAN, J. NEUMAN & W. VAN DRONGELEN – “Wilson–cowan equations for neocortical dynamics”, *The Journal of Mathematical Neuroscience* **6** (2016), no. 1, p. 1.
- [15] G. DECO, V. JIRSA, A. R. MCINTOSH, O. SPORNS & R. KÖTTER – “Key role of coupling, delay, and noise in resting brain fluctuations”, *Proceedings of the National Academy of Sciences* **106** (2009), no. 25, p. 10302–10307.
- [16] G. DECO, V. K. JIRSA & A. R. MCINTOSH – “Emerging concepts for the dynamical organization of resting-state activity in the brain”, *Nature Reviews Neuroscience* **12** (2011), no. 1, p. 43.
- [17] G. DECO, M. L. KRINGELBACH, V. K. JIRSA & P. RITTER – “The dynamics of resting fluctuations in the brain: metastability and its dynamical cortical core”, *Scientific reports* **7** (2017), no. 1, p. 3095.
- [18] G. DECO, A. PONCE-ALVAREZ, D. MANTINI, G. L. ROMANI, P. HAGMANN & M. CORBETTA – “Resting-state functional connectivity emerges from structurally and dynamically shaped slow linear fluctuations”, *Journal of Neuroscience* **33** (2013), no. 27, p. 11239–11252.
- [19] M. DEMIRTAŞ & G. DECO – “Computational models of dysconnectivity in large-scale resting-state networks”, in *Computational Psychiatry*, Elsevier, 2018, p. 87–116.
- [20] A. ELMOATAZ & P. BUYSSENS – “On the connection between tug-of-war games and nonlocal pdes on graphs”, *Comptes Rendus Mécanique* **345** (2017), no. 3, p. 177–183.
- [21] G. B. ERMENTROUT & J. D. COWAN – “A mathematical theory of visual hallucination patterns”, *Biological cybernetics* **34** (1979), no. 3, p. 137–150.
- [22] F. FREYER, J. A. ROBERTS, R. BECKER, P. A. ROBINSON, P. RITTER & M. BREAKSPEAR – “Biophysical mechanisms of multistability in resting-state cortical rhythms”, *Journal of Neuroscience* **31** (2011), no. 17, p. 6353–6361.
- [23] D. GOTTLIEB & C.-W. SHU – “On the gibbs phenomenon and its resolution”, *SIAM review* **39** (1997), no. 4, p. 644–668.
- [24] E. HEWITT & R. E. HEWITT – “The gibbs-wilbraham phenomenon: an episode in fourier analysis”, *Archive for history of Exact Sciences* **21** (1979), no. 2, p. 129–160.
- [25] R. HINDRIKS & M. J. VAN PUTTEN – “Thalamo-cortical mechanisms underlying changes in amplitude and frequency of human alpha oscillations”, *Neuroimage* **70** (2013), p. 150–163.
- [26] W. HUANG, T. A. BOLTON, J. D. MEDAGLIA, D. S. BASSETT, A. RIBEIRO & D. VAN DE VILLE – “A graph signal processing perspective on functional brain imaging”, *Proceedings of the IEEE* (2018).

- [27] A. N. KHAMBHATI, A. E. SIZEMORE, R. F. BETZEL & D. S. BASSETT – “Modeling and interpreting mesoscale network dynamics”, *Neuroimage* (2017).
- [28] S. LIM, F. RADICCHI, M. P. VAN DEN HEUVEL & O. SPORNS – “Discordant attributes of structural and functional connectivity in a two-layer multiplex network”, *bioRxiv* (2018), p. 273136.
- [29] H. G. MEIJER, T. L. EIASSA, B. KIEWIET, J. F. NEUMAN, C. A. SCHEVON, R. G. EMERSON, R. R. GOODMAN, G. M. MCKHANN, C. J. MARCUCCILLI, A. K. TRYBA et al. – “Modeling focal epileptic activity in the wilson–cowan model with depolarization block”, *The Journal of Mathematical Neuroscience (JMN)* **5** (2015), no. 1, p. 7.
- [30] B. MOHAR, Y. ALAVI, G. CHARTRAND & O. OELLERMANN – “The laplacian spectrum of graphs”, *Graph theory, combinatorics, and applications* **2** (1991), no. 871-898, p. 12.
- [31] E. NEGAHBANI, D. A. STEYN-ROSS, M. L. STEYN-ROSS, M. T. WILSON & J. W. SLEIGH – “Noise-induced precursors of state transitions in the stochastic wilson–cowan model”, *The Journal of Mathematical Neuroscience (JMN)* **5** (2015), no. 1, p. 9.
- [32] D. PINOTSIOS, P. ROBINSON, K. FRISTON et al. – “Neural masses and fields: modeling the dynamics of brain activity”, *Frontiers in computational neuroscience* **8** (2014), p. 149.
- [33] M. W. REIMANN, M. NOLTE, M. SCOLAMIERO, K. TURNER, R. PERIN, G. CHINDEMI, P. DŁOTKO, R. LEVI, K. HESS & H. MARKRAM – “Cliques of neurons bound into cavities provide a missing link between structure and function”, *Frontiers in computational neuroscience* **11** (2017), p. 48.
- [34] P. ROBINSON – “Interrelating anatomical, effective, and functional brain connectivity using propagators and neural field theory”, *Physical Review E* **85** (2012), no. 1, p. 011912.
- [35] P. A. ROBINSON, X. ZHAO, K. M. AQUINO, J. GRIFFITHS, S. SARKAR & G. MEHTA-PANDEJEE – “Eigenmodes of brain activity: neural field theory predictions and comparison with experiment”, *NeuroImage* **142** (2016), p. 79–98.
- [36] D. L. ROWE, P. A. ROBINSON & C. J. RENNIE – “Estimation of neurophysiological parameters from the waking eeg using a biophysical model of brain dynamics”, *Journal of theoretical biology* **231** (2004), no. 3, p. 413–433.
- [37] M. RULE, M. STOFFREGEN & B. ERMENTROUT – “A model for the origin and properties of flicker-induced geometric phosphenes”, *PLoS computational biology* **7** (2011), no. 9, p. e1002158.
- [38] A. SANDRYHAILA & J. M. MOURA – “Discrete signal processing on graphs”, *IEEE transactions on signal processing* **61** (2013), no. 7, p. 1644–1656.
- [39] M. SCHIRNER, A. R. MCINTOSH, V. JIRSA, G. DECO & P. RITTER – “Inferring multi-scale neural mechanisms with brain network modelling”, *Elife* **7** (2018), p. e28927.
- [40] M. L. SCHÖLVINCK, A. MAIER, Q. Y. FRANK, J. H. DUYN & D. A. LEOPOLD – “Neural basis of global resting-state fmri activity”, *Proceedings of the National Academy of Sciences* (2010), p. 200913110.
- [41] D. I. SHUMAN, S. K. NARANG, P. FROSSARD, A. ORTEGA & P. VANDERGHEYNST – “The emerging field of signal processing on graphs: Extending high-dimensional data analysis to networks and other irregular domains”, *IEEE Signal Processing Magazine* **30** (2013), no. 3, p. 83–98.
- [42] A. J. SMOLA & R. KONDOR – “Kernels and regularization on graphs”, in *Learning theory and kernel machines*, Springer, 2003, p. 144–158.
- [43] A. SPIEGLER & V. JIRSA – “Systematic approximations of neural fields through networks of neural masses in the virtual brain”, *Neuroimage* **83** (2013), p. 704–725.
- [44] M. L. STEYN-ROSS, D. A. STEYN-ROSS, J. W. SLEIGH & D. LILEY – “Theoretical electroencephalogram stationary spectrum for a white-noise-driven cortex: evidence for a general anesthetic-induced phase transition”, *Physical Review E* **60** (1999), no. 6, p. 7299.
- [45] S. G. SURAMPUDI, S. NAIK, R. B. SURAMPUDI, V. K. JIRSA, A. SHARMA & D. ROY – “Multiple kernel learning model for relating structural and functional connectivity in the brain”, *Scientific reports* **8** (2018), no. 1, p. 3265.
- [46] D. J. WALES & J. P. DOYE – “Global optimization by basin-hopping and the lowest energy structures of lennard-jones clusters containing up to 110 atoms”, *The Journal of Physical Chemistry A* **101** (1997), no. 28, p. 5111–5116.
- [47] H. R. WILSON & J. D. COWAN – “Excitatory and inhibitory interactions in localized populations of model neurons”, *Biophysical journal* **12** (1972), no. 1, p. 1–24.
- [48] H. R. WILSON & J. D. COWAN – “A mathematical theory of the functional dynamics of cortical and thalamic nervous tissue”, *Kybernetik* **13** (1973), no. 2, p. 55–80.

August 21, 2018

MARCO AQIL, MASTER'S THESIS., SUPERVISOR: RIKKERT HINDRIKS, Vrije Universiteit Amsterdam
 E-mail : m.aqil@student.vu.nl